

A CHANGE IN THE CLUSTER ENVIRONMENTS OF RADIO GALAXIES WITH COSMIC EPOCH

G. J. HILL¹

Institute for Astronomy, University of Hawaii; and University of Texas, McDonald Observatory

AND

S. J. LILLY¹

Institute for Astronomy, University of Hawaii

Received 1989 November 30; accepted 1990 June 25

ABSTRACT

The results of an investigation into the cluster environments of radio galaxies spanning a wide range of radio power within a narrow range of redshift at $z \sim 0.5$ are presented. It is found that about half of the powerful classical double radio sources at $z \sim 0.5$ inhabit rich clusters, even though similar sources avoid such environments at low redshift. It is shown that this change includes not only the most powerful sources, but also sources of moderate power where a direct comparison with low-redshift sources is possible. The lowest power radio galaxies appear to inhabit similar environments at both epochs. In deriving these results, it is shown that the absolute magnitudes of the radio galaxies, and probably also of characteristic L^* galaxies, have not changed significantly since $z \sim 0.5$. The environments of the radio galaxies at $z \sim 0.5$ appear to be similar to those of quasars at similar redshifts studied by Yee and Green. The implications for our understanding of the cosmological evolution of the radio source population are discussed. Finally, it is suggested that an evolving intergalactic medium in rich clusters of galaxies could produce the observed change in cluster environment.

Subject headings: cosmology — galaxies: clustering — quasars — radio sources: galaxies

I. INTRODUCTION

The growing evidence (e.g., Stockton 1978, 1982; Dahari 1984; Hutchings, Crampton, and Campbell 1984; Heckman *et al.* 1984, 1986; MacKenty 1989) that the local environment plays a significant role in the active galaxy phenomenon makes the study of the cluster environments of active galaxies at non-negligible redshifts interesting for two reasons, which are possibly related. First, it may be possible to trace the evolution of the physical conditions in various types of environment by determining which environments are the favored locations of active galaxies at different epochs. Second, by studying changes in the physical conditions around active galaxies, it may be possible to understand some of the causes of the dramatic decline in the numbers of active galaxies that has occurred since the peak at redshifts of order $z \sim 2$. Much of the attention in this field to date has centered on quasars (e.g., Hintzen, Ulvestad, and Owen 1983; Yee and Green 1984, 1987), although some work on limited numbers of radio galaxies has been published (Eales 1985; Yates, Miller, and Peacock 1989). In this paper, we present a study of the cluster environments of about 50 radio galaxies at $z \sim 0.5$.

It has long been known that extragalactic radio sources (both radio galaxies and quasars) have undergone drastic evolution in comoving number density (e.g., Longair 1966). Analysis of multifrequency source-count data and the redshifts of the identifications in selected samples have led to successful characterization of the form of the radio source population evolution (e.g., Peacock 1985), but very little progress has been made toward a physical explanation for this phenomenon. Viewed in terms of the epoch-dependent radio luminosity func-

tion (RLF), there is marked differential evolution of the radio source population (RSP) in the sense that the RLF at high power has changed to a much greater degree than at low power (Longair 1966). This is illustrated in Figure 1. The RLFs at $z = 0$ and $z = 0.5$ are derived from Peacock's (1985) model 1, for rest frame radio powers between 10^{24} and 10^{28} W Hz⁻¹ at rest frame 2.0 GHz. The RLF above the break at $10^{25.3}$ W Hz⁻¹ shows a greater increase in comoving space density with increasing power, reaching factors greater than 10 at $z = 0.5$ for powers $> 10^{27}$ W Hz⁻¹. The RLF below the break shows little or no evolution between these epochs. For reference, the powers of the well-known low-redshift radio galaxies Cygnus A and Centaurus A are indicated on Figure 1. Straightforward comparison of the RLFs at the different epochs provides some constraints on the type of evolution allowed but cannot distinguish between the physically distinct scenarios of luminosity evolution, differential density evolution, or a combination of the two.

The properties of low-redshift radio galaxies have been studied in some detail. Fanaroff and Riley (1974) demonstrated a marked change in the radio structure of double-lobed sources at powers close to that of the break in the radio luminosity function and introduced a widely used classification scheme. Below the break, radio structures are often distorted and show strong central regions of surface brightness, fading into extended "edge-darkened" lobes. Such sources are designated FR I. Above the RLF break, the objects are usually "classical double" sources with the regions of highest surface brightness occurring in hotspots at the outer extremes of the lobes and are designated FR II. A further refinement of the classification scheme was proposed by Longair and Riley (1979), who subdivided the FR II sources into "good," "doubtful," and "not good" depending on the visibility of the hotspots.

¹ National Radio Astronomy Observatory Visiting Astronomer. The NRAO is operated by Associated Universities, Inc., under contract with the National Science Foundation.

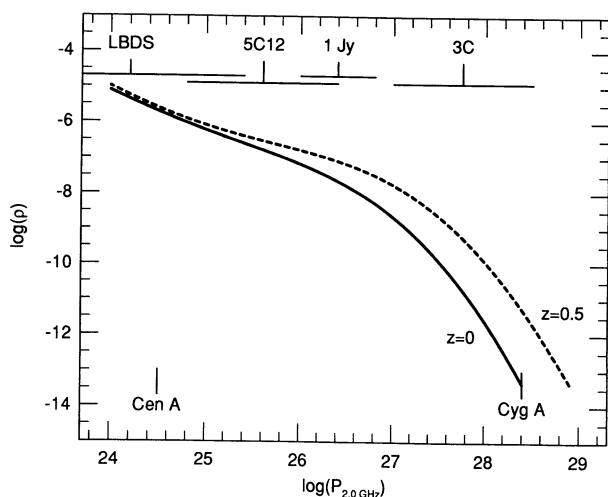


FIG. 1.—The radio luminosity functions at rest frame 2.0 GHz for $z \sim 0$ and $z \sim 0.5$ from Peacock (1985). The luminosities of the local sources Centaurus A and Cygnus A, and the range of luminosities present in the various subsamples at $z = 0.5$, are shown.

Subsequent studies of the optical properties of radio galaxies have demonstrated quite marked differences between FR I and FR II sources, and, equivalently, between high- and low-power sources. At low redshift, the low-power FR I sources usually inhabit moderately rich cluster environments (Longair and Seldner 1979; Prestage and Peacock 1988, 1989, hereafter together PP), in which they are the first-ranked ellipticals (Sandage 1973; Lilly and Prestage 1987; Owen and Laing 1989). They show little nuclear emission-line activity (Hine and Longair 1979). The more powerful “classical double” FR II sources found above the RLF break are associated with slightly less luminous, smaller, but more optically active galaxies which are either isolated or are the dominant galaxies in small groups of sub-Abell richness. Heckman *et al.* (1986) and Smith and Heckman (1989) present evidence that the host galaxies of FR II sources may be more disturbed or peculiar than those which host FR I radio morphologies. The existence of long-lived differences (such as the cluster environments and the stellar luminosities of the host galaxies between high-power FR II and low-power FR I sources at the current epoch is important because it indicates that sources cannot evolve between these classifications on the time scales of individual radio sources ($\sim 10^7$ yr). Taken together, these trends imply an intimate connection between the environment and the physics of the radio structure and possibly with the initial triggering of the nuclear activity.

The differences between the cluster environments of weak FR I sources and more powerful FR II sources are thought (see, e.g., PP) to be due to the increased pressure of the intergalactic medium in the richer environments. This may prevent the formation of classical double lobe structure in rich environments, except in sources of very high beam power, such as Cygnus A, which is thought to inhabit a fairly rich environment (Spinrad and Stauffer 1982). More typical sources in rich clusters may suffer severe jet disruption and correspondingly only attain low radio luminosities and FR I structure.

It is to be hoped that the evolution of the radio source population (RSP) may in some way be linked to changes in some other readily observable properties of the host galaxies or their environments, although, if we are unlucky, it could be entirely hidden in the poorly understood physics of the central

engine. One possibility for an observable cause is the evolution of the gaseous content of elliptical galaxies, perhaps manifested as an evolving star-formation rate (see, e.g., Lilly and Longair 1984). The aim of this paper is to investigate the possibility that changes in the cluster environments may be playing a major role. The cluster environments of a large sample of radio galaxies at $z \sim 0.5$ are studied and compared with those of low-redshift radio galaxies.

A key feature of the present study is the selection, from several different flux density-limited samples, of a large sample of radio galaxies that span a wide range of radio power (10^4) within a narrow range of redshift centered on $z = 0.45$. The range of powers present in the high-redshift sample is shown in Figure 1. Sources in the sample cover the entire range from Centaurus A to Cygnus A. This epoch around $z \sim 0.5$ was chosen as it is the highest redshift at which it is currently possible to assemble such a sample, and yet the space density evolution of the RSP is already significant. This is also an epoch at which significant evolutionary phenomena in cluster galaxies have been observed (e.g., Butcher and Oemler 1978). Indeed, the cluster associated with the radio galaxy 3C 295 ($z = 0.46$) was one of the first to show the Butcher-Oemler effect, and one of the motivations of this project is to determine how typical 3C 295 is of other radio galaxies at the same epoch. Evolutionary effects *within* the sample are effectively eliminated due to the relatively narrow range of redshift, allowing the independent investigation of correlations between radio power and other properties. Epoch-dependent changes are studied through the comparison of the properties of the $z \sim 0.5$ sample with those of sources of the *same* power at low redshift. This unambiguously separates the two quantities which are so closely correlated in flux density-limited samples. The choice of essentially a single redshift for the high-redshift sample also offers considerable simplifications in the execution of the program, allowing a single observational set-up to be used yet still producing data in a single rest frame waveband with uniform spatial coverage.

The paper is arranged as follows: an account of the construction of the sample, the observations, and data reduction is presented in § II, along with a discussion of the choice and implementation of a clustering parameter. Results concerning the cluster luminosity function and the radio galaxy Hubble diagram are also included here. In § III, the principal results are presented and discussed, while § IV is a summary. Cosmological parameters of $H_0 = 50 \text{ km s}^{-1} \text{ Mpc}^{-1}$ and $q_0 = 0.5$ are assumed throughout, although the effects of the assumed geometry are discussed where relevant.

II. OBSERVATIONS AND ANALYSIS

a) Sample Selection

The $z \sim 0.5$ sample is drawn from the northern hemisphere 3CR samples of Laing, Riley, and Longair (1983) and Spinrad *et al.* (1985), the “1 Jy” B2 sample of Allington-Smith and colleagues (Allington-Smith, Lilly, and Longair 1985 and Allington-Smith *et al.* 1988), the 5C12 sample of Benn *et al.* (1988), and the Leiden-Berkeley Deep Survey (LBDS) millijansky sample of Windhorst, Kron, and Koo (1984). The basic sample consists of radio galaxies from these samples with redshifts between $z = 0.35$ and 0.55 , galactic reddening less than $A_V = 0.15$, $08^h < \text{R.A.} < 18^h$, and declinations less than 70° . The total sample of 45 radio galaxies was supplemented by six quasars from the above surveys which had redshifts between

0.4 and 0.5. Because there are ~ 10 objects in each of the four flux density-limited samples, the radio luminosities are roughly evenly spread through a 10^4 range in power.

The 3C and "1 Jy" parts of the sample are essentially complete in the sense that we can be fairly confident that no objects have been excluded on account of their optical brightness. The 3C sample has been completely identified, and redshifts have been obtained for essentially all sources (Spinrad *et al.* 1985). The "1 Jy" sample has been completely identified (see, e.g., Lilly 1989), and redshifts are now available (Allington-Smith *et al.* 1988) to a limiting magnitude well below those of the $z = 0.5$ radio galaxies in this sample. We can be confident that the remaining sources have $z \gg 0.5$. The situation in the two fainter samples is less satisfactory. The 11 5C12 sources were originally selected on the basis of photometrically estimated redshifts, based on v magnitudes and $v - r$ colors (from Benn *et al.* 1988), to have $0.35 < z_{\text{est}} < 0.6$. Subsequent spectroscopy (see below) has in all cases confirmed that the photometric redshifts are good estimates of the spectroscopic redshifts, and the fact that the average difference $z_{\text{est}} - z_{\text{spect}} = -0.004 \pm 0.015$ suggests that the absolute magnitudes of the radio galaxies in this subsample are probably not systematically biased. Finally, the LBDS sample consists of all LBDS sources with spectroscopic redshifts (from Windhorst, Kron, and Koo 1984 and private communications) in the required range that have $(J - F) > 0.2F - 0.24$ (Kron, Koo, and Windhorst 1985). The color criterion was applied to avoid the population of blue galaxies which appears in faint mJy radio surveys. These galaxies cause an upturn in the radio number counts, but do not show double radio structure and may not be true "radio galaxies" (Kron, Koo, and Windhorst 1985; Oort *et al.* 1987). While the LBDS sample could in principle be biased against intrinsically fainter galaxies, we believe that this is unlikely. In any case, subsequent analysis of the remainder of the sample (see below) suggests that there is not a strong correlation between absolute magnitude and the richness of the cluster environment, so the cluster richness measurement should not be biased even in the presence of a weak bias in absolute magnitude. Table 1 presents the photometric and radio properties of the sample.

In order to make a comparison between the high- and low-redshift epochs to study evolutionary effects, it is necessary for the low-redshift sample to have high-resolution radio maps, accurate photometry, and measures of galaxy clustering around each radio source. These constraints combine to yield a fairly limited number of sources, all selected from the work of Prestage and Peacock (1988, 1989). PP measured the spatial covariance amplitude B_{gg^*} between galaxies, g , and radio galaxies, g^* , (e.g., Longair and Seldner 1979) for a sample of radio galaxies from the Parkes Bright Survey (Peacock and Wall 1981), the 2.7 GHz Parkes Survey (Wall 1977), and two 5 GHz surveys (Kühr *et al.* 1981). The sample was constrained to have good radio maps to classify the radio morphology and to lie at $z < 0.15$. The Lick galaxy counts (Shane and Wirtanen 1967; Seldner *et al.* 1977) in the photographic blue were used to calculate B_{gg^*} , and the redshift limit was imposed due to the relatively bright limiting magnitude of that data. In addition a small number of higher redshift, more powerful sources were included, for which PP calculated values of B_{gg^*} from deeper UK Schmidt J plates. PP used the counts of galaxies within 1 Mpc radius of the radio galaxies and normalized to the average galaxy counts within annuli located between 3° and 5° , corresponding to a distance of around 13–22 Mpc at the mean

redshift $z = 0.045$ of their sample. The sample contains 77 sources with a range of radio powers between $\log(P_{2.7 \text{ GHz}}) = 24$ and 27 W Hz^{-1} . Surface photometry of a subsample of 23 of the PP radio galaxies was obtained by Lilly and Prestage (1987) in a study of correlations between the optical and radio properties of radio galaxies.

b) Optical Imaging Observations

Deep, wide-field R band CCD imaging of the fields of 43 of the radio galaxies and four of the quasars in the sample was obtained at the UH 2.2 m telescope between 1987 January and 1988 March. As discussed above, low-redshift clustering studies have generally been undertaken in the photographic blue, so the R band was chosen for the present study as it is close to the rest frame B band at $z \sim 0.5$. This reduces the need for precise K -corrections and/or knowledge of the mix of galaxy Hubble types, etc., in the analysis. For each object, one, or occasionally more, comparison fields located $30'$ (12 Mpc at $z \sim 0.45$) away were also observed for the same amount of time under the same observing conditions. This separation between the object and comparison fields is thus comparable to that used by PP for the low-redshift sample. The comparison field positions were chosen to avoid clusters from the Zwicky catalog (Zwicky *et al.* 1961–1968), which would contaminate the comparison field number counts. The "1 Jy" source 1025 + 34 ($z = 0.361$) was excluded due to insufficient observing time, and 53W046 ($z = 0.545$) was mistakenly not observed.

A number of CCD and focal-reducer combinations were used at the $f/10$ Cassegrain focus of the University of Hawaii 2.2 m reflector, giving plate scales of $0''.59\text{--}0''.9 \text{ pixel}^{-1}$, and usable fields of view of $5'\text{--}6'$, or 2.0–2.5 Mpc at $z = 0.45$. For each observation, the total integrations of between 15 and 30 minutes were split into several 2–5 minute exposures. The telescope was rastered by about $10''$ between exposures to improve sampling and to allow sky flat fields to be generated from the data. About 75% of the data was obtained with thinned TI 500×500 or 800×800 pixel CCDs, while the remainder used a thick GEC 576×385 pixel CCD which suffered from a higher cosmic-ray detection rate. All the CCDs were low-noise devices (six to 15 electrons) and had quantum efficiencies of between 40% and 75% at R . The two focal reducers were designed by A. N. Stockton and were used with a reduction factor of about five for all the observations. Photometric calibration was achieved with observations of equatorial standards from Landolt (1983). Mean extinction terms were obtained for each observing run, and mean color corrections were obtained for each CCD and focal-reducer combination. All the data were obtained at air masses less than 1.5.

i) Imaging Data Reduction

Reduction of the CCD data was standard. The bias was subtracted from individual frames which were then flattened with dome flats. Dark counts were found to be negligible for these short integration times. The dome flats removed most of the pixel-to-pixel nonuniformity of the CCD chips but left some large-scale structure due to nonuniform illumination and differences in color between the sky and flat-field lamp. The frames were further flattened by dividing by a sky flat-field frame. The sky flats were generated by taking the median response of each pixel after normalizing the modes of the frames to a standard sky value. Frames containing bright stars or very extended objects were not used in this procedure. A

TABLE 1
 $z \sim 0.5$ SAMPLE PHOTOMETRIC AND RADIO PROPERTIES

Object	z	$m_{R,tot}$	$M_{B,tot}$	$M_{B,1.4\gamma}$	Radio Structure ^a	$\log(P_{2.0\text{GHz}})$ (W Hz ⁻¹)
3C 200	0.458	19.17	-22.15	-22.05	II d	27.2
3C 215Q ^{b,c}	0.425	18.00	-24.75	-24.75	II n	27.0
3C 228	0.5524	20.34	-21.71	-21.55	II g	27.6
3C 244.1	0.428	18.65	-22.39	-22.10	II g	27.4
3C 268.3	0.371	19.69	-20.91	-20.80	II g	27.3
3C 274.1	0.422	19.11	-21.88	-21.68	II g	27.3
3C 275	0.48	19.74	-21.74	-21.48	II g	27.5
3C 295	0.4614	17.78	-23.52	-23.00	II g	28.2
3C 299 ^c	0.367	18.55	-22.02	-21.88	C	27.1
3C 306.1	0.441	18.60	-22.65	-22.29	II g	27.1
3C 313	0.461	18.78	-22.56	-22.26	II g	27.4
3C 330	0.549	19.51	-22.54	-22.42	II g	27.9
3C 341	0.448	18.89	-22.40	-21.98	II g	27.2
0822+34A	0.406	19.13	-21.81	-21.68	II n	26.6
0835+37	0.396	19.62	-21.24	-21.26	C	26.3
0847+37 ^b	0.407	18.72	-22.20	-22.03	II d	26.5
0854+39A	0.528	19.35	-22.32	-22.08	II g	26.7
1104+36 ^c	0.393	17.72	-23.05	-23.05	II d	26.6
1130+34	0.512	19.72	-22.00	-21.75	II g	26.7
1201+39	0.445	19.35	-21.82	-21.74	II g	26.6
1216-010Q	0.415	18.89	-22.06	-22.06	C	26.1
1220+37Q	0.489	18.06	-23.47	-23.47	II g	26.6
1245+34	0.42	19.13	-21.85	-21.80	II g	26.4
1301+38A	0.47	19.11	-22.26	-22.02	II g	26.7
5C12 71	0.436	19.40	-21.70	-21.52	I	24.8
5C12 75	(0.64)	20.29	-22.45	-22.34	II d	25.5
5C12 91	0.464	18.85	-22.47	-22.26	II n	25.4
5C12 142	(0.65)	19.88	-22.94	-22.37	II g	25.2
5C12 168	0.424	18.76	-22.25	-21.88	I	25.5
5C12 217	0.428	19.52	-21.52	-21.33	II g	25.6
5C12 235	(0.66)	20.39	-22.51	-22.34	II n	25.8
5C12 241 ^b	0.487	19.83	-21.68	-21.58	II d	26.4
5C12 264	0.373	18.33	-22.29	-21.83	C	25.6
5C12 287	0.583	19.75	-22.54	-22.05	I	25.7
5C12 304	0.460	19.57	-21.72	-21.33	C	25.8
53W032	0.37	18.20	-22.42	-22.31	I?	24.7
53W039	0.402	18.56	-22.30	-22.02	I?	24.3
53W076	0.39	18.74	-22.03	-21.83	I?	23.9
53W079	0.548	19.99	-22.04	-21.81	C	25.1
55W010	0.452	18.60	-22.67	-22.44	C	25.4
55W016	0.375	19.19	-21.48	-21.45	I?	24.5
55W023	0.36	18.35	-22.21	-22.06	I?	24.3
55W097	0.365	19.78	-20.82	-20.70	I?	23.6
55W150	0.465	20.17	-21.20	-21.00	I?	23.8
55W161B	0.402	19.49	-21.38	-21.29	I?	23.9
55W173Q	0.45	20.32	-20.93	-20.93	I?	24.4
0841+444	0.425	19.62	-21.43	-21.34	I?	23.4

^a See text for explanation.

^b Extended diffuse 20 cm emission detected with B-array.

^c Blue ($R-K$) colors indicate presence of nonthermal nuclear emission.

separate sky flat was generated for each night. All data frames were then divided by the appropriate sky flat, and this effectively divided out the original dome flat which was just used to obtain a first-order flattening of the frames.

Registration of the frames for each field was achieved by calculating the mean shift in the centroids of 10 stars on each frame. A fractional pixel shift was performed by linear interpolation. Due to the presence of often low-level cosmic-ray events, the median rather than the mean of the registered frames was calculated. The final frames were flat to better than 0.5% and often better than 0.2% of sky. There is a danger in using the median, that flux will not be conserved where surface brightness is changing rapidly. This effect was studied by comparing stellar and galaxy aperture magnitudes in averaged

frames, with those where the median was calculated. There was no systematic difference in the magnitudes. Stars in the final frames all had profiles with FWHM of about 1".5, due to seeing.

The final stage in the frame reduction was to remove cosmetic defects. Low-level halos around bright stars and saturation trails tend to be recognized as large numbers of spurious objects by image recognition algorithms, and these were removed. Halos were associated with saturated stars and were quite symmetrical. These were removed by subtracting the median radial profile above the modal sky level. The central regions of the saturated stars, where the surface brightness was changing rapidly, were masked out. Row and column saturation streaks were also masked out. While these procedures

produced a dramatic improvement in the appearance of the frames, it should be noted that the effected pixels only account for a few percent of the total area and thus do not significantly affect the number-count statistics of the frame.

ii) Image Recognition

The program MULTIM, available as part of the GASP reduction package (see Davis *et al.* 1985), was used for image recognition. MULTIM analyzes the data for connected images with total counts larger than a specified minimum and pixel values above a set of thresholds. Since the detection of faint extended objects, where individual pixel values in the image may be significantly below 3σ for the sky, is of prime importance for the present investigation, the lowest level was taken as 1σ above the sky. Subsequent higher levels were placed at 0.5σ increments, until 5σ above the sky, after which the threshold levels increased as a square law. Twenty-five levels were used, and objects found at any single level were included in the source list if their total counts were greater than or equal to a certain fixed level (set to 5 times the dispersion in the sky pixel values).

Empirically, MULTIM was very successful in finding all objects visible on the frames plus many more, so it is likely that all real objects were identified. Since such low threshold levels were used, MULTIM naturally found many spurious sources, but these were subsequently filtered out in a controlled manner. The output from the program consists of positions and sizes and was filtered to remove objects with areas of 1 pixel, since these were invariably due to noise in the sky coupled with the 1σ lower threshold used. No systematic differences in the identification statistics were discernible in the regions close to bright stars or close to masked regions. Careful inspection of each frame showed that no visually discernible objects had been missed.

iii) Photometry

The resulting list of positions and sizes was fed to a multi-object photometry program which returned growth curves and aperture and isophotal magnitudes for each object in the list. The operation of the photometry program was straightforward. A subarray about $50''$ on a side was extracted centered on the object to be measured. The local sky value was found by determining the mode of the pixels in this box. All objects except the one being measured were then masked out of the subarray for the photometry. The surface brightness distribution and growth curve of the object were generated from the median of the pixels at a given radius, except within $2''$ radius where instead the average was taken due to the rapidly changing surface brightness. The median has a great advantage in cases where there are nearby objects which would distort the surface brightness distribution even after they had been masked out. It is not possible to entirely remove the effects of such cases, but the above approach significantly reduces their distortion of the photometry.

Objects were rejected as unmeasurable if their centers were within $2''$ of one another, or within $2''$ of the edge of the frame or a masked region. Very few objects were rejected due to overlapping images, and in such cases they were considered as one object. Since this typically affected only one pair of objects per frame out of many hundreds, this procedure had a negligible effect on the results. Isophotal magnitudes were calculated from the growth curves, correcting for masked areas. There was found to be a negligible difference in the magnitudes of isolated objects when this procedure was compared to a simple

sum of the pixel values within the isophotal radius. In cases where the isophotal radius was less than $1''.5$, the magnitude within $1''.5$ radius was used instead. This avoids the tendency to undercount faint galaxies when an isophotal magnitude is employed (see, e.g., Tyson 1988). The $R = 27.5$ mag arcsec $^{-2}$ isophote was chosen because the resulting magnitudes were within about 0.2 of the total magnitudes. Total magnitudes were not used as they are too sensitive to uncertainties in the local sky level. The photometry is dominated by errors in the sky level, which result in random errors of ~ 0.1 mag at $R \sim 23$. Figure 2 shows the isophotal apertures and magnitudes used for two arbitrarily selected frames. The typical apertures used at $R = 23$ were $5''$ – $6''$ in diameter.

It should be emphasized that the radio galaxy and comparison field frames were treated identically throughout the reduction, to ensure against the introduction of systematic errors. No star-galaxy separation was attempted in this investigation, as galaxies dominate the number counts at magnitudes fainter than $R \sim 20$ (see Fig. 4), and the comparison fields should sample the same stellar surface density as that in the radio galaxy fields. Accurate star-galaxy separation at faint magnitudes is difficult, and the potential for introducing systematic uncertainties outweighs any benefits to be gained from such an analysis of the present data.

c) Radio Mapping Observations

Radio continuum snapshot observations were obtained at the VLA. The A and B configurations were used at wavelengths of 6 and 20 cm to obtain maps with typically $1''.4$ and $4''.2$ (FWHM) resolution. The 20 cm A array observations were made on UT 1987 July 23, 28 and 29, while the 6 and 20 cm B array observations were obtained on UT 1987 November 15 and 17. Most of the reduction of the radio data was done at the VLA site with standard calibration software and with the AIPS software package. The data were calibrated relative to the standards 3C 48 and 3C 268. Clean maps were made and the 3C and "1 Jy" sources were self-calibrated to produce dynamic ranges of greater than 100.

These data were used to classify the radio structure following the scheme of Fanaroff and Riley (1974). Table 1 gives the adopted classifications. The classification scheme compares the separation of radio flux density maxima (hot spots) in the radio

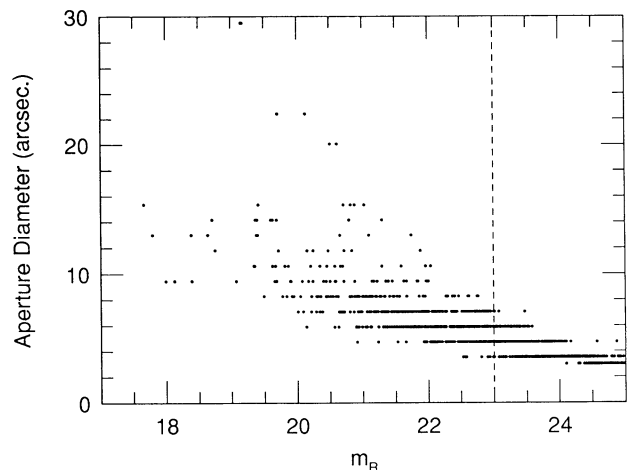


FIG. 2.—Isophotal apertures and magnitudes. The vertical dashed line represents the limiting magnitude adopted for these data, which are from two randomly selected frames.

lobes with the total extent of the radio emission. Sources with hot spot separations greater than half the total source extent are classified as FR II, while the regions of most intense emission in FR I sources are closer to the center. It was decided to separate the FR II sources into "good" classical doubles (IIg; Longair and Riley 1979) which have well-defined single hot spots in each lobe collinear with the galaxy or quasar, and "other" (II_d, II_n) FR II sources with ill-defined or missing hot spots or bent radio structure. Sources dominated by a compact core are denoted by "C" in the table.

Obviously the classification depends somewhat on the resolution and quality of the radio observations, and in a comparison between sources at high and low redshift, it is important that the data be of sufficient quality so as not to misclassify objects in a redshift-dependent way. The maps obtained of the brighter sources in the sample (3C, "1 Jy", and most of the 5C) are often of higher dynamic range than those available for the sources in the low-redshift comparison sample of PP, and the classification is straightforward. For the low-redshift comparison sample, the structure classifications of PP have been adopted after checking the original references. The new VLA observations of the fainter 5C12 and the LBDS sources were of sufficient duration (10–15 minutes) to detect hot spots in the lobes or core sources if most of the flux density of the sources was concentrated in such features. If a compact core or hot spots were detected, a reliable classification can be made; otherwise, it is assumed that FR I morphology is most likely, and these sources are classed as FR I? in Table 1. Given the limitations of observing time and the number of sources involved, this approach yields the best classification possible, and the maps are often not significantly worse than those available for the low-redshift sources.

It is important to consider whether FR I sources have been classified as FR II due to the nondetection of faint emission extending beyond hot spots in the lobes. This question was addressed by comparing the high-resolution ($\sim 1''.2$) A array 20 cm maps with the lower resolution ($\sim 4''.2$) B array maps. Observations with the larger beam are sensitive to large, low surface brightness regions which may have been missed in the higher resolution data. In a few cases, more extended emission was detected, and this is noted in Table 1. However, given the quality of the maps, it is unlikely that any source with power greater than the radio luminosity function break (at $\log(P_{2.0 \text{ GHz, rest}}) = 25.3 \text{ W Hz}^{-1}$) has been misclassified.

d) Spectroscopy of 5C12 Sources

Identifications and finding charts for the 5C12 sources in the sample were kindly supplied by C. R. Benn in advance of publication. Spectroscopic observations of the 5C12 sources were obtained at the University of Hawaii 2.2 m telescope with the UH Faint Object Spectrograph (FOS) and at the McDonald Observatory 2.7 m telescope with the Large Cassegrain Spectrograph (LCS). Both instruments used thinned TI 800 \times 800

CCDs as detectors, and the resolutions were between about 16 and 20 Å. Details of the observations are given in Table 2. The FOS was used with a 2" slit, an 85 mm camera lens, and a 600 lines mm^{-1} grating, to give a dispersion of 3 Å pixel^{-1} . The seeing was about 1''.5 and the data were binned 2×2 on the CCD to improve signal-to-noise ratio. The LCS was used with a 300 lines mm^{-1} grating to give 3.4 Å pixel^{-1} dispersion. Slit widths of 3"–6" were used depending on the seeing which ranged from 1''.5 to 4" and the data were binned by a factor of 2 or 4 in the spatial direction. Spectrophotometric standards from Stone (1977) and Oke and Gunn (1983) were used to correct for the system response. Integration times are given in Table 3 for each object. The wavelength ranges are also noted in the table.

The basic reduction of the data was standard. The VISTA data reduction package (Stover 1988) was used. The LCS data suffer from large amplitude (up to 20% of sky) fringing longward of 7500 Å, and flats were taken between each exposure without moving the telescope in order to minimize the effects of flexure on the fringe pattern. Even so, the sky subtraction was sometimes poor in this region of the spectra. Cosmic rays were interactively removed from regions away from the spectra and the affected pixels replaced with the median of surrounding pixels. Slight tilts in the spectra relative to the rows of the CCD were removed. An optimal extraction scheme (Horne 1986) was used to obtain the highest possible signal-to-noise ratio. The sky-subtracted spectra so obtained were compared with those obtained simply by co-adding the data over a spatial region significantly larger than the extent of the galaxy, to ensure that the optimal extraction preserved the shape of the continuum. The spectra were linearized using argon comparison spectra and corrected for atmospheric absorption and instrumental system response. The data were not flux-calibrated as they were obtained under nonphotometric conditions and, in the case of some of the McDonald data, had poor seeing.

Redshifts were obtained from the [O II] $\lambda 3727$ and [O III] $\lambda 5007$ emission lines, where present, but usually no emission line was evident, and absorption-line redshifts were measured from the Ca II H and K lines, the G band at $\lambda 4304$, and the CN feature at $\lambda 3885$. The lines used and their observed wavelengths and redshifts are given in Table 3, together with the adopted redshifts. The redshifts of three of the sources need confirming observations, and these are noted in the table. These three objects have tentative redshifts of $z \sim 0.65$, which are consistent with the estimated redshifts inferred from photometry.

e) Cluster Richness Measure

i) Choice of Cluster Parameterization

Two measures of cluster richness have been used extensively at low redshift. The Abell richness class (Abell 1958), based on

TABLE 2
SUMMARY OF SPECTROSCOPIC OBSERVATIONS

UT Date	Telescope	Instrument	Dispersion (Å pixel^{-1})	Resolution (Å)	Seeing
1988 Feb 19–20	UH 2.2 m	FOS	3.0	20	1''.5
1989 Mar 9–12	McD 2.7 m	LCS	3.4	16	2
1989 Apr 8, 11	McD 2.7 m	LCS	3.4	16	2–4
1989 Jun 4–5	McD 2.7 m	LCS	3.4	16	1.5

TABLE 3
SPECTROSCOPY OF 5C12 RADIO GALAXIES

Object	UT Date	Exposure (s)	Wavelength Coverage (Å)	Line ID	λ (Å)	z	Adopted Redshift
5C12 71	1989 Mar 10	12000	5210–7930	K	5648	0.4357	0.436 ± 0.002
	1989 Apr 11	6600	5235–7955	H	5695	0.4352	
				G	6182	0.4363	
5C12 75	1988 Feb 20	5400	4670–7040	[O II]?	6110	0.64	$0.64 \pm 0.01?$
5C12 91	1988 Feb 19	3600	4670–7040	K	5758	0.4637	0.464 ± 0.002
	1989 Mar 11	9000	4880–7600	H	5808	0.4637	
				G	6295	0.4626	
5C12 142	1988 Feb 20	7200	4670–7040	K?	6478	0.647	$0.65 \pm 0.01?$
	1989 Mar 12	9000	5480–8100	H?	6544	0.649	
				G?	7082	0.646	
5C12 168	1988 Feb 19	4500	4670–7040	[O II]	5308	0.4242	0.4243 ± 0.0005
				H	5652	0.4244	
				G	6130	0.4243	
5C12 217	1989 Mar 9	6100	4980–7710	[O II]	5311	0.425	0.428 ± 0.007
				[O III]	7170	0.432	
				[Ne III]	5522	0.427	
5C12 235	1989 Mar 12	3600	5480–8100	[O II]?	6196	0.663	$0.662 \pm 0.005?$
				CN?	6463	0.664	
				K?	6533	0.661	
				H?	6595	0.662	
5C12 241	1988 Feb 19	4200	4670–7040	[O II]	5544	0.4875	0.487 ± 0.003
	1989 Jun 6	11880	5385–8115	K	5845	0.4858	
				H	5898	0.4864	
				G	6400	0.4870	
5C12 264	1989 Apr 8	28350	4885–7605	K	5403	0.3734	0.373 ± 0.003
				H	5452	0.3740	
				G	5905	0.3720	
5C12 287	1989 Jun 5	9000	5350–8075	[O II]	5898	0.5825	0.583 ± 0.001
				K	6225	0.5824	
				H	6278	0.5822	
5C12 304	1989 Jun 4	9000	5385–8115	K	5775	0.4680	0.464 ± 0.003
				H	5808	0.4637	
				G	6290	0.4615	

the number of objects within 3 Mpc radius and brighter than $m_3 + 2$ (where m_3 is the apparent magnitude of the third brightest cluster member) is a very simple, robust quantity. A more quantitative, though less direct, measure of the degree of clustering around a point in space is the amplitude B_{gg}^2 of the spatial covariance function (e.g., Seldner and Peebles 1978). This has been used in studies of radio galaxy environments at low redshift (Longair and Seldner 1977; PP) and, at higher redshift ($z \sim 0.5$), in studies of quasar environments (Yee and Green 1984, 1987) and previous, less extensive studies of radio galaxy environments at redshifts up to $z \sim 0.5$ (Yates, Miller, and Peacock 1989; Eales 1985). The correlation statistic approach has particular merit when the limiting magnitude of the galaxy catalog is fixed and/or the magnitudes of the individual galaxies are unknown, as in the case of the Lick counts. In practice, the derivation of B_{gg} at high redshift is often based on straightforward number counts of galaxies on small field-of-view CCD frames, so the two methods are not that distinct operationally. The advantage and simultaneously the drawback of B_{gg} is that it is referenced to the general galaxy luminosity function. Consequently, its derivation requires that the form of the galaxy luminosity function be known as a function

² B_{gg} will be used to denote the amplitude of the spatial covariance function, except in the specific case of the radio galaxies, where B_{gg^*} will be used.

of redshift. Unfortunately, the luminosity function is poorly constrained at $z \sim 0.5$, since it is sensitive to ill-constrained evolutionary and cosmological parameters. Furthermore, reference to an absolute luminosity function requires that the galaxy photometry be carried out in exactly the same way at each redshift. Consequently, comparisons between high- and low-redshift measurements are difficult.

In the case of radio galaxies, but unfortunately not for quasars, these difficulties can be alleviated to a certain degree by adopting a cluster richness measurement similar to that of Abell, in which the measurements of the cluster galaxies are referenced to that of the radio galaxy, assumed to be the first-ranked member. This procedure will eliminate first-order effects related to the not inconsiderable problems of faint galaxy photometry, and, if it is assumed that the stellar population evolution of the radio galaxies and typical cluster galaxies is similar, then the epoch dependence of the luminosity function is also dealt with. Aside from second-order correction terms, the redshift of the radio galaxy enters into the analysis only to fix the sampling radius within which galaxies are to be counted, which is not a strong function of redshift at $z \sim 0.5$. In passing, it should be noted that while recent results on the evolution of cluster galaxies (Butcher and Oemler 1984) and radio galaxies (Lilly and Longair 1984) might make the assumption of similar evolution for all cluster members a ques-

tionable one, both the radio galaxies and the majority of the members of rich clusters at this redshift have the optical-infrared colors of quiescent elliptical galaxies (see, e.g., Lilly 1987).

In the same way that Yee and Green (1987) attempted to remove the evolutionary ambiguities involved in deriving B_{gg} by an empirical determination of the luminosity function of the galaxies that were statistically associated with their quasars, we can also check that the evolution of the cluster galaxies is the same as that inferred for the radio galaxies, and this is done below. One potential problem with an Abell-type measurement is that it could become highly nonlinear in a very poor environment if the galaxies were selected from a normal Schechter-type luminosity function, since both m_1 and m_3 would be strong functions of the number of galaxies. This is not the case with radio galaxies since the absolute magnitudes of radio galaxies are not a strong function of the richness of the environment (LP, see also below). Even radio galaxies that appear to be completely isolated are almost as luminous as the first-ranked galaxies in rich clusters.

We believe that there are considerable operational advantages to the use of an Abell-type measurement and have adopted this approach in our study. We define a quantity $N_{0.5}$ which is the net excess number of galaxies within 0.5 Mpc radius of the radio galaxy within a magnitude range m_1 to $m_1 + 3$, where m_1 is the magnitude of the radio galaxy. The advantages of this approach are primarily in its robustness and insensitivity to some of the uncertainties which can affect the alternative analysis, but the two are, in principle, equivalent. Unfortunately, PP's analysis of low-redshift radio galaxies was based primarily on the Lick counts, so an Abell-type measurement is not recoverable from their raw data. Until equivalent measurements are obtained for low-redshift radio galaxies, our choice of an Abell-type of analysis for the high-redshift sample requires us to obtain a calibration between the two forms of measurement. Both $N_{0.5}$ and B_{gg} should be linear functions of the astrophysically interesting density around the radio galaxy, and so the problem reduces to finding the constant of proportionality between them. This can be done in the low-redshift regime where both are potentially easily determined. The calibration is achieved (see below) empirically through PP's measurements of B_{gg} for Abell clusters as a function of richness class, coupled with Bahcall's (1981) determinations of the numbers of galaxies within 0.5 Mpc in similar clusters. This empirical calibration is shown to be consistent with an ab initio calculation.

Because of the difficulty of identifying the third brightest cluster member at $z \sim 0.5$ (due to the high statistical background contamination), we have adopted an $m_1 + 3$ magnitude range rather than the $m_3 + 2$ conventionally used by Abell. Even in rich environments, $m_1 + 3$ is brighter than $m_3 + 2$. In terms of metric aperture magnitudes, $m_1 + 3$ is generally about 0.4 mag brighter than $m_3 + 2$, and in terms of a total magnitude, the difference is about 0.8 mag (Schneider, Gunn, and Hoessel 1983). Hence use of $m_1 + 3$ will lead to a (conservative) underestimation of the cluster environments. The size of this shortfall may be as large as 20%–30%. Because of the background contamination, we have counted galaxies within a 0.5 Mpc rather than a 3 Mpc radius. In the case of the four quasars and also 1104+36 and 3C 299, whose $R-K$ colors indicate that they contain significant nonstellar nuclear emission, we adopted the mean m_1-z relation for the sample.

ii) Calibration of $N_{0.5}$ and B_{gg}

The large Poisson uncertainties that are involved in determining the richnesses of clusters at high redshift due to the high degree of contamination mean that only crude statements of cluster richness are meaningful. For an individual object at $z \sim 0.5$, the Poisson uncertainty corresponds to roughly an Abell richness class, and the present study is primarily aimed at saying whether radio galaxies are in Abell-type clusters or not, given that at low redshift, powerful sources are definitely found in much poorer environments. The accuracy of the $N_{0.5}$ - B_{gg} calibration is most important for clusters of Abell richness. We approach this calibration in two ways.

Bahcall (1981) gives values of $N_{0.5}$ corrected for the observed variation of m_3 with cluster richness, for 23 Abell richness class 0, 1, and 2 clusters. The mean values of $N_{0.5}$ for these Abell clusters as a function of richness class are shown in Table 4. It should be noted that, empirically the luminosities of radio galaxies show very little systematic variation with the richness of their environment (see § III, below), and thus the radio galaxy magnitude may be taken statistically as a fixed point on the cluster-galaxy luminosity function. As a result the values of $N_{0.5}$ calculated for the $z \sim 0.5$ sample are already referenced to a fixed luminosity range, comparable to that employed by Bahcall in the calculation of the corrected $N_{0.5}$ values for Abell clusters. As noted above, the $z \sim 0.5$ richnesses probably involve a smaller portion of the galaxy luminosity function and are thus likely to be underestimates relative to the values of Bahcall. Along with their measurements of radio galaxies, PP measured B_{gg} values for a sample of 107 Abell clusters. The mean values for each richness class are also shown in Table 4 and graphically compared with the $N_{0.5}$ values in Figure 3. A weighted least-squares linear fit was made between the two quantities giving $B_{gg} = 30 N_{0.5}$. Mean $N_{0.5}$ values for Abell clusters were determined from the closest approach of the above fit to the $N_{0.5}$ - B_{gg} data points to be 10, 19, and 31 for richness classes 0, 1, and 2, respectively.

One can also perform an ab initio calibration of B_{gg} and $N_{0.5}$ in terms of the basic definition of B_{gg} as the amplitude of the spatial correlation statistic $\xi(r)$ at 1 Mpc. To maintain consistency with PP, we take a Schechter luminosity function with $M_B^* = -21.0$ and $\alpha = -1.25$ and integrate this over the 3 mag range below each radio galaxy's absolute magnitude. The radio galaxies have an average $M_B = -22.2$ (see below). With a normalization $\phi^* = 0.0022 \text{ Mpc}^{-3}$, this yields an average of 0.0036 galaxies Mpc^{-3} . Integrating over the density function $\rho(r) = B_{gg} r^{-1.77}$ gives an "effective volume" within a cylinder of radius 0.5 Mpc of $8.3 B_{gg} \text{ Mpc}^3$ for an $r^{-1.77}$ profile. Consequently, with the same parameters as used by PP, the calculated calibration is $B_{gg} = 34 N_{0.5}$. This is also shown on Figure

TABLE 4
 B_{gg} - $N_{0.5}$ CALIBRATION

Richness	$\langle B_{gg} \rangle$	σ	$\langle N_{0.5} \rangle$	σ
0	288	30	12	3
1	690	72	15	5
2	985	121	29	8
Mean 3C	249	129	11	2
Median 3C	291	...	10	...

NOTE.—Mean and median 3C values are calculated from the data of Yates *et al.* 1989. See text for details.

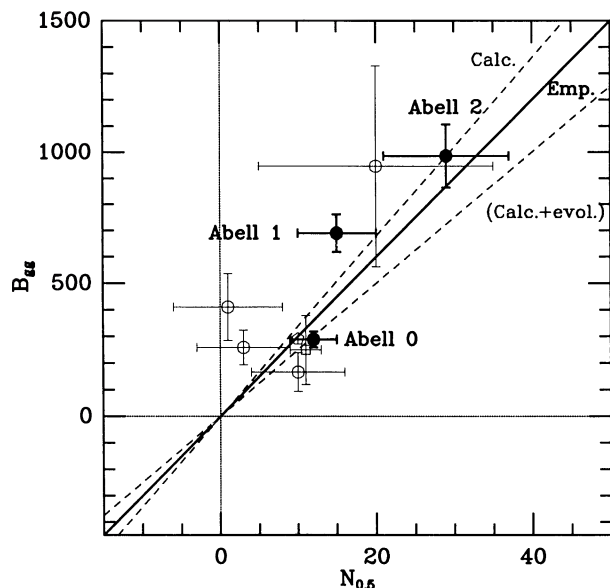


FIG. 3.—The calibration of $N_{0.5}$ and B_{gg} . Solid points represent mean values for Abell clusters of indicated Abell class, and the heavy line represents the (adopted) best-fitting linear relation. Light data points represent four 3C radio galaxies at $z \sim 0.5$ observed by both Yates *et al.* (1989) and ourselves. The square point is the mean of the Yates *et al.* (1989) 3C objects, and the pentagon is the median (see Table 4). The dashed line represents a theoretical non-evolving calibration. Some of the discrepancy, which is in the sense of $N_{0.5}$ underestimating the cluster richnesses, is due to the different counting methods of Bahcall (1981) and ourselves (see text). The effect of adding either a 0.5 mag evolutionary brightening in L^* or a 30% increase in ϕ^* is shown.

3. The small discrepancy between this calibration and the empirical calibration above is in the sense that use of the former will *underestimate* the richness of the high-redshift clusters (measured with $N_{0.5}$) when compared with the low-redshift clusters (measured with B_{gg}). The discrepancy is accounted for by the difference between $m_1 + 3$ and $m_3 + 2$ discussed above.

The relevance of the theoretical calibration to the high-redshift sample is of course open to considerable question, since we might expect galaxy evolution to have altered the form of the luminosity function between now and $z \sim 0.5$. Current interpretations of the Butcher-Oemler effect (see e.g., Dressler, Gunn, and Schneider 1985) involve some substantial brightening of at least some fraction (around 25%) of the galaxies in clusters at $z \sim 0.5$, and the basic number counts of field galaxies also show an excess at $B \sim 22$ of about 30% (see Ellis 1983). If galaxies were brighter or more numerous in the past, as these arguments indicate, then the theoretical calibration of B_{gg} and $N_{0.5}$ would change. We will return to this point in § IIe(iv) below, where we derive the observed luminosity function in our high-redshift clusters.

iii) Determination of $N_{0.5}$

For each object and comparison field, number counts as a function of magnitude were constructed. The limiting magnitude of each image was defined to be 0.5 mag brighter than the peak of the number-magnitude histogram. In all cases this was very similar for the two object and comparison fields. Figure 4 presents the mean number counts (*solid line*) from all 13 comparison fields obtained with the TI 800 \times 800 CCD, indicating the limiting magnitude adopted. The points show the effect of the corrections described above, and the error bars indicate the standard deviation of the mean for each point. The measured R band number counts of Tyson (1988) which closely follow

$\log(N) = 0.39R - 4.80$, are indicated by a dashed line for comparison. The contribution from stars is indicated by the dotted line. These data are from Bahcall and Soneira (1984) for the north Galactic pole region, taking $(V-R) = 0.4$. Nine of the fields have $b > 50^\circ$ and all have $b > 35^\circ$, and the Galactic pole field counts agree well with the data. As can be seen from the figure, stars dominate the number counts at magnitudes brighter than $R \sim 20$.

Small corrections were applied to account for incompleteness close to the limiting magnitude, without regard to whether the image was an object or comparison field. The multiplicative correction as a function of magnitude was calculated such that application of the correction would result in the comparison field number counts following an extrapolation of the power-law fit to the data between $R = 21$ and 0.5 mag brighter than the limiting magnitude. Separate corrections were generated for the mean comparison field counts of each observing run. A more complicated approach is not warranted since the limiting magnitudes for fields from a given observing run show little variation. The net excess number of galaxies, $N_{0.5}$ as defined above, over that from the relevant comparison field(s), was calculated. For 15 objects, another multiplicative factor was applied to $N_{0.5}$, when the limiting magnitude of the image was brighter than $m_1 + 3$. This factor is defined to be $\Phi(m_1 + 3)/\Phi(m_{lim})$, where $\Phi(m)$ is the integral number of galaxies brighter than magnitude m . A Schechter (1976) luminosity function with $\alpha = -1.25$ and $M_B^* = -21.0$ was assumed. K -corrections were taken from Coleman, Wu, and Weedman (1980), and a rest frame $B-R$ color of 1.8 was adopted. Due to rather bright limiting magnitudes, the total corrections for 3C 228, 1130+34, and 5C12 235 were greater than a factor of 2. As a result, the richnesses were rather uncertain for these objects and they were not considered further in the analysis. The corrections were $< 10\%$ for five of the objects, $> 10\%$ for seven of them. The random Poisson errors in the counts are of

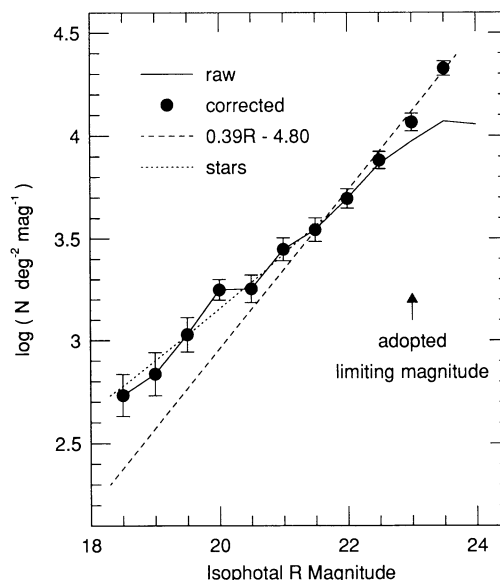


FIG. 4.—Comparison field number counts as a function of R magnitude. The observed $0.39R - 4.80$ line for galaxies is from Tyson (1988), while the stellar number counts are from Bahcall and Soneira (1984). The solid line represents the raw data, and the solid points, the corrections applied for incompleteness (see text). The error bars show the standard deviation on the mean points.

order seven to 10 objects and are essentially independent of $N_{0.5}$. Values of raw and corrected $N_{0.5}$ are presented in Table 5 together with the Poisson uncertainty. The total correction factor applied to each value of $N_{0.5}$ is given in column (13) of the table. Values of $N_{1.0}$, the corrected number of objects within 1 Mpc radius, and its uncertainty are also presented in this table. For comparison, column (10) gives the corrected $N_{0.5}^M$ values when the mean m_R - z relation for the radio galaxies is used as m_1 , instead of the magnitudes of the radio galaxies.

There is no difference in the results if $N_{0.5}^M$ is used rather than $N_{0.5}$. The individual values change, but by much less than the 1σ errors given in Table 5.

In addition to these basic number counts, a spatial correlation statistic ζ provides an independent measure of the number of galaxies at small projected radii from the radio galaxy, compared to the number which would be expected if all the objects in the field were distributed at random. Only objects brighter than the limiting magnitude and fainter than

TABLE 5
CLUSTER RICHNESS MEASURES

Object (1)	z (2)	m_R (3)	m_{lim} (4)	$N_{0.5} R$ (5)	$N_{0.5}$ (6)	$\sigma_{0.5}$ (7)	$N_{1.0}$ (8)	$\sigma_{1.0}$ (9)	$N_{0.5}^M$ (10)	$N_{0.5}^0$ (11)	ζ (12)	f_c (13)
3C 200	0.458	19.19	22.5	2	2	6	9	12	2	1	0.62	1
3C 215	0.411	18.03	22.5	21	21	6	57	11	37	16	4.20	1
3C 228	0.5524	20.36	22.5	8	20	15	99	33	18	25	-0.02	2.54
3C 244.1	0.428	18.67	22.3	15	15	7	2	11	15	15	6.26	1
3C 274.1	0.422	19.15	22	9	10	6	28	11	7	9	1.58	1.08
3C 268.3	0.371	19.75	23	16	16	9	49	17	13	11	-0.42	1.01
3C 275	0.48	19.81	23	1	1	7	18	15	2	1	0.46	1.09
3C 295	0.4614	17.83	22	10	10	5	6	9	29	8	7.73	1
3C 299	0.367	18.48	23	2	2	5	5	10	2	3	0.60	1
3C 306.1	0.441	18.59	23	3	3	6	-5	12	5	3	0.33	1
3C 313	0.461	18.84	23	16	16	7	23	12	22	14	7.58	1
3C 330	0.549	19.5	23	18	18	7	48	14	20	18	3.68	1
3C 341	0.448	18.94	22	7	7	7	20	13	10	5	1.03	0.97
0822+34A	0.406	19.16	22.5	5	5	8	19	15	7	1	-1.95	1
0835+37	0.396	19.41	23	32	32	9	57	17	19	25	5.49	1
0847+37	0.407	18.74	22	16	16	7	45	13	17	15	3.10	1
0854+39A	0.528	19.35	22.5	10	10	7	14	14	10	8	3.19	1
1104+36	0.393	17.72	22	3	3	4	8	7	10	3	0.94	1
1130+34	0.512	19.96	22.2	21	45	8	125	15	46	39	1.41	2.14
1201+39	0.445	19.37	22.5	8	8	7	12	14	7	8	2.25	1
1216-010	0.415	18.93	22	-8	-8	5	-6	12	-7	-5	-1.10	1.02
1220+37	0.489	18.07	22.5	2	2	5	-7	8	18	1	2.20	1
1245+34	0.42	19.17	22.3	18	18	7	25	13	13	18	3.63	1
1301+38A	0.47	19.22	22.5	2	2	7	1	14	1	1	0.51	1
5C12 71	0.436	19.46	23	12	12	7	62	15	13	8	-1.92	1
5C12 75	0.64	20.3	23	27	39	12	127	22	35	33	1.57	1.47
5C12 91	0.464	18.85	23	15	15	6	38	12	18	13	3.09	1
5C12 142	0.65	19.94	23	36	37	9	82	15	32	32	4.75	1.03
5C12 168	0.424	18.78	22	1	1	5	-1	10	1	3	0.76	1
5C12 217	0.428	19.54	23	11	11	7	30	14	6	7	0.70	1.02
5C12 235	0.66	20.39	22.5	16	46	17	38	31	34	33	2.21	2.79
5C12 241	0.487	19.83	23	11	12	8	20	14	9	8	1.13	1.09
5C12 264	0.373	18.41	23	6	6	5	13	10	4	6	2.12	1
5C12 287	0.583	19.87	23	5	5	8	26	14	4	7	1.72	1.10
5C12 304	0.46	19.57	23	25	26	8	81	15	22	22	1.16	1.01
53W032	0.37	18.24	22	6	6	6	16	11	7	8	1.32	1
53W039	0.402	18.59	22.5	11	11	6	17	12	12	10	2.91	1
53W076	0.39	18.84	21.5	10	11	7	31	13	11	11	0.35	1.09
53W079	0.548	20.03	23	25	26	8	65	16	23	18	0.43	1.01
55W010	0.452	18.64	22.5	5	5	6	0	10	5	5	0.54	1
55W016	0.375	19.23	21.8	2	2	8	23	17	-1	0	-0.48	1.28
55W023	0.36	18.37	22	-1	-1	5	45	12	-2	1	-2.28	1
55W097	0.365	19.89	22	14	21	11	35	20	15	21	2.06	1.52
55W150	0.465	20.39	22.6	3	5	14	11	25	1	8	2.55	1.94
55W161	0.402	19.54	22	2	2	9	-22	18	-3	4	1.85	1.49
55W173	0.45	20.43	22	-2	-4	10	-15	20	2	-9	-0.96	1.98
0841+444	0.425	19.73	22	-8	-14	9	-18	19	-15	-13	-1.57	1.72

COL. (5).—Raw count of excess objects within a radius of 0.5 Mpc for $q_0 = 0.5$.

COL. (6).—Corrected value.

COL. (7).—Its error (see text for details).

COLS. (8) and (9).—Equivalent values for a 1 Mpc radius.

COL. (10).—Corrected value of $N_{0.5}$ for the case where the mean m_R - z relation of the sample is used as a fixed point on the galaxy luminosity function.

COL. (11).—Corrected value for $q_0 = 0$.

COL. (12).—Correlation statistic.

COL. (13).—Total correction factor applied to the raw $N_{0.5}$ data; see text for details.

the radio galaxy were considered. The statistic is the sum, over all those objects that met the above criteria, of

$$\zeta = \sum_{n=1}^{N(<1 \text{ Mpc})} e^{-r/\alpha} - 0.07677 N_{1,\text{tot}},$$

where α is chosen such that the peak response to a uniform surface density distribution occurs at a radius of 0.2 Mpc, and the half-response point is at 0.55 Mpc. This results in objects within 0.5 Mpc contributing overwhelmingly to ζ . The summation includes all $N_{1,\text{tot}}$ objects within 1 Mpc of the radio galaxy. The normalization is provided by calculating the same statistic for the case where all the $N_{1,\text{tot}}$ objects are distributed uniformly over the region. The value of ζ is roughly proportional to the excess number of galaxies distributed within about 0.5 Mpc but also reflects the tightness of their distribution around the radio galaxy. Thus, the spatial correlation statistic measures the degree of clustering around the radio sources independent of the comparison field data, providing a valuable check of the richnesses derived. Values of ζ are presented in Table 5. $N_{0.5}$, $N_{1.0}$, and ζ are of course interrelated.

Figure 5 illustrates the relationship between the quantities $N_{1.0}$, $N_{0.5}$, and ζ for the radio galaxies in the sample. The scatter of values close to the origin is entirely consistent with the 1σ errors deduced from Poisson statistics. The majority of the fields lie away from the origin, and many evidently have real and often rather rich clusters presumably associated with the radio galaxies. Fields with negative values of ζ are indicated by filled circles, those with $0 < \zeta < 2$ by open circles, and those with $\zeta > 2$ are represented by triangles. As expected, most fields with $\zeta > 2$ lie significantly to the right of the locus of $N_{1.0} = 4N_{0.5}$ which is indicated by a dashed line, indicating an excess of galaxies clustered preferentially around the radio galaxy position. On the other hand, all but one of the $\zeta < 0$ fields lie to the left of the $N_{1.0} = 4N_{0.5}$ line. Fields with positive

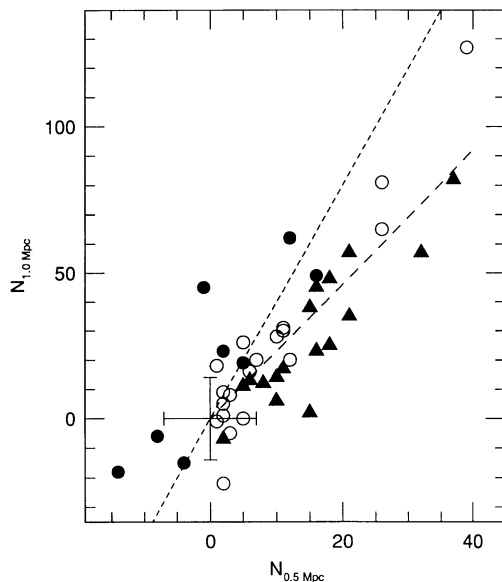


FIG. 5.—Cluster richnesses measured within 1 Mpc radius ($N_{1.0}$) compared with those within 0.5 Mpc ($N_{0.5}$). Solid circles have values of the correlation statistic $\zeta < 0$, open circles have $0 < \zeta < 2$, and triangles have $\zeta > 2$ (see text for details). The two lines represent the loci of $N_{1.0} = 4N_{0.5}$ and $N_{1.0} = 2.3N_{0.5}$, the latter appropriate for a $\theta^{-0.8}$ surface density profile. The error bars show the typical 1σ errors due to counting statistics and are independent of richness.

N , but with ζ less than or equal to zero and $N_{1.0} \approx 4N_{0.5}$, are presumably false clusters caused by mismatched comparison fields. There are quite wide ($\sim 50\%$) variations in the number counts between comparison fields, consistent with that noted by other authors (e.g., Ellis 1983), but such mismatching should cancel out statistically within a reasonably sized sample. The object 3C 244.1 is probably a case where the comparison field has higher counts than it should, since it has $N_{1.0} = 2$, even though visual inspection shows an obvious cluster, and the object has large $N_{0.5}$ and ζ values. It should be emphasized that determinations of B_{gg} at comparable redshift (e.g., Yee and Green 1987; Yates, Miller, and Peacock 1989) use similar data and will suffer from the same random effects. The data are quite consistent with the $N_{1.0} = 2.3N_{0.5}$ expected if the surface density of galaxies falls off as $\theta^{-0.8}$. This is important since the B_{gg} values for the low-redshift sample of PP are determined at 1 Mpc sampling radius.

iv) The Hubble Diagram and Cluster Galaxy Luminosity Function

A further check of the reality of the clusters detected and their true association with the radio sources is to look at the luminosity function implied for the galaxies associated with the clusters (e.g., Yee and Green 1987). These galaxies should have the same redshift as the radio galaxies. The distribution of rest frame B band absolute magnitudes of the excess galaxies found within 0.5 Mpc of the radio galaxy were computed for each of the 12 radio galaxy clusters that had $z \leq 0.55$, values of the correlation statistic $\zeta > 2.0$ and $N_{0.5} > 10$, and that had overall incompleteness corrections of less than 10%. Small differential K -corrections (for an elliptical spectral energy distribution from Coleman, Wu, and Weedman 1980) were applied so as to bring the observed R band onto the rest frame B band in the calculation of the absolute magnitudes. The luminosity distributions were then binned in 0.1 mag intervals down to $M_B = -19.0$, which is above our standard $R = 23$ limit for all redshifts below 0.55. Nevertheless, two of the 12 clusters (3C 295 and 0854 + 39A) were incomplete at this level, due to brighter limiting magnitudes $R < 23$ in the R band images, and these clusters were subsequently excluded from the analysis. The distributions of the remaining 10 clusters are all complete to $M_B \leq -19.0$. They were normalized to an arbitrary $N_{0.5}$ and then averaged, and errors were calculated assuming Poisson statistics for the uncertainty in the original object and comparison field counts. Schechter (1976) luminosity functions with the normalization and the value of M_B^* as free parameters were fitted to the 0.1 mag binned luminosity function over the range $-19 < M_B < -24$, so as to minimize χ^2 . For the assumed $\alpha = -1.25$, the best-fitting luminosity function has $M_B^* = -20.90 \pm 0.4$ for $q_0 = 0.5$ (or -21.15 for $q_0 = 0.0$). The resulting luminosity function for $H_0 = 50$ and $q_0 = 0.5$ is shown in Figure 6, binned in 0.5 mag intervals. The fit is indicated on the figure by a solid line, while the $\pm 1\sigma$ fits are dashed lines.

The 0.1 mag binned points on the luminosity function with $-19 \leq M_B < -19.5$ have had a correction of about 7% applied to them (see Fig. 4 and the discussion in § IIe[iii]). The effect of this correction on the derived value of M_B^* has been explored by not applying any correction and by applying twice the correction to the data. Both of these have a negligible effect (less than 0.1 mag) on the answer. Similarly, if the error bars on these faintest points are doubled, the resultant M_B^* changes only to -20.80 , and a similar value is derived if the points below -19.5 are omitted entirely. Finally, if the two incom-

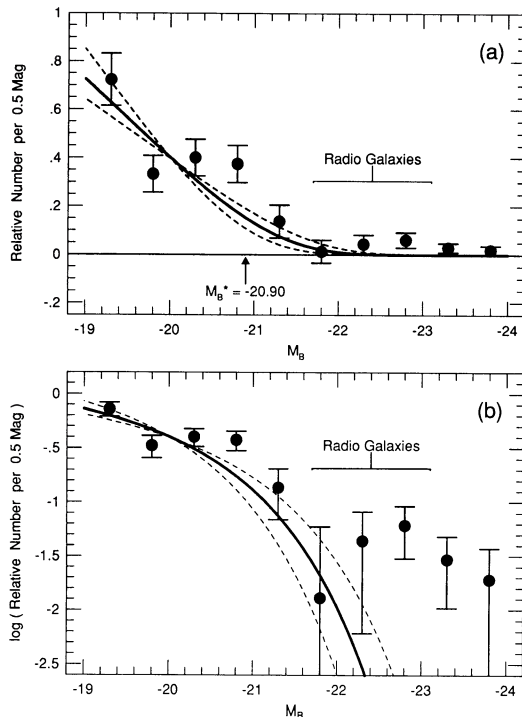


FIG. 6.—The cluster galaxy luminosity function of the 10 most certain clusters associated with $z \sim 0.5$ radio sources in (a) linear and (b) logarithmic forms. The best-fitting Schechter luminosity function with $M_B^* = -20.90$, and the $\pm 1 \sigma$ fits are indicated by solid and dashed lines respectively. The $\pm 1 \sigma$ range of radio galaxy magnitudes is also indicated.

plete fields are included for luminosities above their incompleteness level, the value changes insignificantly to $M_B^* = -20.75$. The derived value of M_B^* is thus insensitive to the incompleteness correction applied to the data and it is not possible to change the derived value of M_B^* by more than about half the formal uncertainty by changing the errors or corrections.

This analysis suggests that at $z \sim 0.5$, the luminosity of an L^* galaxy in these clusters has not changed significantly from the value of $M_B^* \sim -21.0$ found with $\alpha \sim -1.25$ at low redshift (see, e.g., Felton 1977; King and Ellis 1985). The derived luminosity function thus supports the assumption that the excess galaxies are at the same redshift as the radio sources, providing a check that they are indeed in clusters associated with the radio galaxies and quasars.

The bright end of the luminosity function provides another check on systematic errors. The fact that there is no net excess of objects at luminosities $M_B > -23$ provides a further important check for systematic errors in the measured cluster richnesses. The fields which have a galaxy excess relative to the comparison field do not exhibit that excess at levels brighter than the radio galaxy. As discussed above, it is possible for such systematic errors to occur for individual sources, but Figure 6 shows that this does not cause a systematic error when the statistical properties of the sample are considered. The slight excess at $M_B \sim -22.7$ is due to the radio galaxies themselves. The $\pm 1 \sigma$ range of the magnitudes of the 10 radio galaxies is indicated on the figure. As at low redshift (LP), the radio galaxies themselves are not selected from the Schechter function of their associated clusters. It should be noted that the radio galaxies do not perturb the luminosity function analysis

of the previous paragraphs, as similar results are obtained if points brightward of $M_B = -22.0$ are omitted.

Absolute metric B magnitudes of the radio galaxies in the $z \sim 0.5$ sample and the low-redshift sample of Lilly and Prestage (1987) were calculated for an aperture of radius $1.4\gamma = 26.9$ kpc. $\gamma = 19.2h^{-1}$ kpc (where $H_0 = 50h$ km s $^{-1}$ Mpc $^{-1}$), as defined by Gunn and Oke (1975). This aperture was chosen as a compromise between minimizing aperture corrections for the low-redshift objects (for which magnitudes in apertures of radius γ are given by LP) and avoiding possible seeing effects in smaller apertures for the higher redshift sample. Magnitudes within this aperture were directly measured for the $z \sim 0.5$ galaxies. The low-redshift data were aperture corrected to $r = 1.4\gamma$ assuming the surface brightness distributions of the galaxies could be described by a de Vaucouleurs profile (e.g., de Vaucouleurs and Capaccioli 1979). For this purpose, measurements of the Gunn-Oke structure parameter α_γ given in LP were transformed to values of the effective radius r_e via

$$r_e = 10^{(\alpha_\gamma + 0.18)/0.58}$$

(Lilly, McLean, and Longair 1984). The low-redshift galaxies have the well-defined colors of old stellar populations allowing a reliable correction from observed R to B magnitudes assuming $B - R = 1.80$ (Coleman, Wu, and Weedman 1980). The absolute magnitude versus redshift diagram for the radio galaxies is presented in Figure 7. The $z \sim 0.5$ sample galaxies are divided into groups depending on the sample from which they were originally selected (i.e., by radio power). This diagram shows no systematic variation of absolute magnitude with radio power or the initial sample from which the source was selected. This should allay worries that the 5C and LBDS portions of the sample are biased towards intrinsically more luminous galaxies.

There is clearly little evidence for a large change in the rest frame B absolute magnitudes of the radio galaxies out to $z = 0.5$. Formally, the mean absolute magnitude brightens from $M_B = -21.71 \pm 0.15$ to $M_B = -21.79 \pm 0.08$, an insignificant change. This lack of evolution to $z = 0.5$ is in agreement with longer wavelength infrared photometry (Lilly and

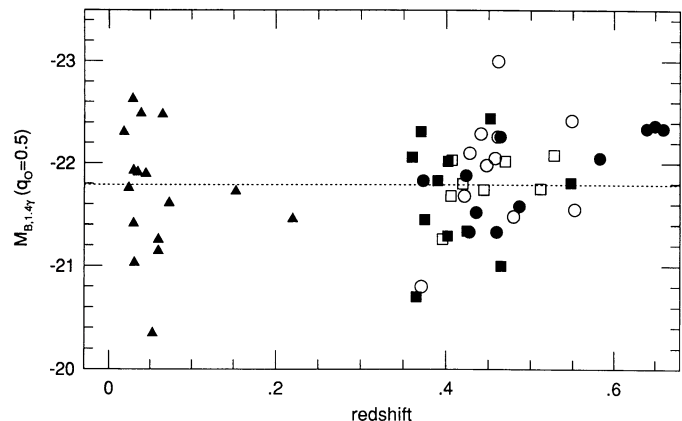


FIG. 7.—The absolute metric B magnitudes of the high- and low-redshift radio galaxies as a function of redshift. The symbols for the $z \sim 0.5$ sample denote the different samples from which the objects were drawn: open circles are 3C, open squares are "1 Jy," filled circles are 5C12, and filled squares are LBDS galaxies. The dashed line has $M_B = -21.79$, the mean for the $z \sim 0.5$ galaxies. There is little evidence for evolution between $z \sim 0.5$ and the present, for $q_0 = 0.5$.

Longair 1984; Lilly 1989). Coupled with the lack of evolution in L^* that was found above, this supports the use of the radio galaxy magnitude to define an epoch-invariant point on the luminosity function that is the basis of our Abell-type cluster parameterization.

The lack of strong evolution in the characteristic M_B^* and in the radio galaxies themselves is also consistent with recent spectroscopic surveys of faint field galaxies down to $B = 21.5$ (Broadhurst, Ellis, and Shanks 1988) and $B = 22.5$ (Colless *et al.* 1990). Despite the fact that the number counts of field galaxies are well in excess of no-evolution predictions, these surveys found a median redshift close to that expected in the no-evolution case and failed to find large numbers of luminous galaxies at $z > 0.5$. This indicates little evolution in the luminosities of present-day L^* galaxies but requires an effective increase in ϕ^* caused, it is thought, by brightening of sub- L^* galaxies up to L^* brightnesses. The steep source counts to $B = 22.5$ at least are therefore not caused by uniform brightening of galaxies in the past, but by a differential effect only operating on low-luminosity systems.

Yee and Green (1987) have however claimed to see substantial evolution ($\Delta M_B^* \sim 0.5 \pm 0.5$ mag) in L^* within the clusters associated with their quasars out to $z \sim 0.5$ and derived self-consistent models for galaxy evolution and cosmology that simultaneously accounted for this change in M_B^* and for the observed number counts of galaxies in their comparison fields. Yee and Green's normalization has also subsequently been used by Yates, Miller, and Peacock (1989). H. K. C. Yee (private communication) finds similar evolution to Yee and Green (1987) but with a factor of 2 smaller error from deeper imaging data. The cause of this discrepancy is not known. The adoption of a luminosity function at $z \sim 0.5$ that had brightened by 0.5 mag would change the theoretical calibration between $N_{0.5}$ and B_{gg} described above by about 35%, to $B_{gg} = 25 N_{0.5}$. The effects of galaxy evolution will be further discussed in § IIe(v).

Direct comparison can be made in the cases of the four 3C galaxies observed by both Yates, Miller, and Peacock (1989) and in this work. These have been plotted on Figure 3. There is good qualitative agreement in that 3C 228 is found by both groups to lie in a rich cluster, and the quantitative agreement on this object is also satisfactory, although unfortunately it is the object with the largest correction applied in our sample. There is also satisfactory overall agreement between the average B_{gg}^* values of Yates *et al.*'s eight radio galaxies with $0.35 < z < 0.55$ and the $N_{0.5}$ values of our significantly larger and largely independent 3C sample. These sample comparisons are included in Table 4.

v) Systematic Uncertainties

There are additional sources of systematic uncertainty in this work which should be discussed. Incorrect choice of q_0 leads to an incorrect 0.5 Mpc radius sampling area on the sky, but not, in this formulation, to an incorrect sampling of the luminosity function. Changing to $q_0 = 0$ leads to an overestimate of 14% in the angular size of the 0.5 Mpc area, and hence, with a $\theta^{-0.8}$ angular dependence of surface density, to a 15% overestimate in richness. Reanalysis of the data for $q_0 = 0$ (Table 5, col. [11]) shows that indeed the determined richnesses decrease by this amount. This uncertainty is sufficiently small as to be negligible.

The sampling radius used in this analysis is of fixed metric size, rather than a comoving size. This is of course appropriate

for virialized systems. Yates, Miller, and Peacock (1989) have discussed the effect of considering nonvirialized structure fixed in comoving space. For $\xi \propto r^{-1.8}$, the richness at $z = 0.5$ is overestimated by a factor of $(1+z)^{1.2}$, or about 1.55. As will be seen below, this is approaching the change seen in the average richness of clusters at $z \sim 0.5$ (a factor of 2.5). We believe that adoption of this scenario would be quite extreme and do not entertain it further.

Finally, we return to the luminosity function of the cluster galaxies, which remains a fundamental uncertainty in work of this kind. While we believe (see above) that there is little evidence for a systematic brightening in L^* at $z \sim 0.5$ and our analysis technique would in any case have been insensitive to such a change, ϕ^* could have been effectively increased if low-luminosity galaxies were preferentially brightened sufficiently to reach L^* luminosities in a similar way to what appears to be happening in the field (see the discussion above). Although it is quite possible for cluster and field galaxies to evolve differently, an obvious candidate is the Butcher-Oemler effect, which is now thought (e.g., Dressler, Gunn, and Schneider 1985; Lavery and Henry 1988) to be caused by bursts of star formation and their aftermath. However, the fraction of galaxies undergoing the Butcher-Oemler effect at $z = 0.5$ is still quite small (blue fractions ~ 0.25 – 0.3 ; Butcher and Oemler 1984) and the majority of cluster members have the colors of normal elliptical galaxies, certainly in the rest frame UVH colors (Lilly 1987). A 30% overestimation in density could arise from this effect since ϕ^* would be effectively 30% larger. Note that this is of the same order as the effect of a 0.5 mag brightening of the luminosity function in the B_{gg} calibration. Consequently, even though we believe that L^* has not brightened back to $z \sim 0.5$ (see above) as claimed by Yee and Green (1987), their evolutionary calibration of B_{gg} would actually "correct" for this potential effect. Given our safety margin already incorporated into the B_{gg} - $N_{0.5}$ calibration (because of the difference between $m_1 + 3$ and $m_3 + 2$), this corrected calibration is still within 20% of our empirical unevolving calibration (see Fig. 3). The $N_{0.5}$ values presented in Table 5 are thus only about 20% higher than they would be if the parameterization of the galaxy luminosity function evolution of Yee and Green (1987) were adopted and accounted for. Thus evolution of L^* or ϕ^* , if present, will not change the results significantly.

III. RESULTS AND DISCUSSION

a) Cluster Richness, Radio Power, and Structure

Figure 8a presents the cluster richness $N_{0.5}$ as a function of radio power for the $z \sim 0.5$ sample, and Figure 8b presents the corresponding low-redshift data from PP. The radio powers are calculated at a rest frequency of 2.0 GHz. While the high-redshift sample contains many more very high power sources, there is a considerable degree of overlap for $\log(P_{2.0}) < 27$ W Hz $^{-1}$, in the range spanning the break in the RLF at $\log(P_{2.0}) \sim 25.3$ W Hz $^{-1}$. This is particularly true in the critical decade above the break.

The most striking difference between the two epochs is that FR II radio sources often inhabit rich-cluster environments at $z \sim 0.5$ but almost totally avoid them at low redshift. Considering all FR II sources in the low- and high-redshift samples, a single-tailed Mann-Whitney U -test (Mann and Whitney 1974) shows that the distribution of $N_{0.5}$ at $z \sim 0.5$ extends to much richer environments than at low redshift. This result is very significant ($> 99.99\%$ confidence).

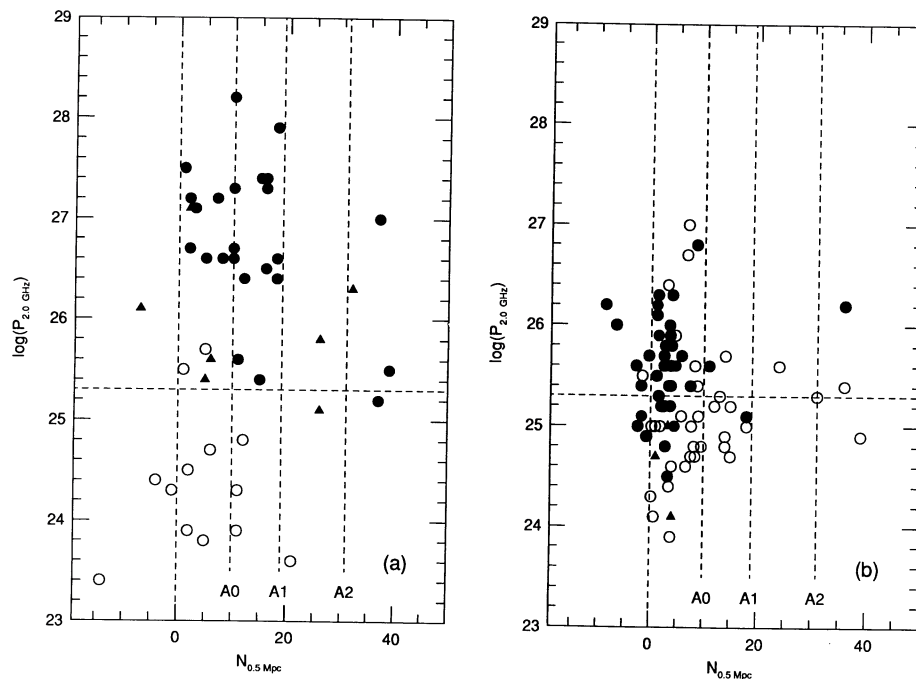


FIG. 8.—Cluster richness $N_{0.5}$ as a function of rest-frame 2.0 GHz radio power for (a) the $z \sim 0.5$ sample, and (b) the $z \sim 0$ sample. The symbols denote the radio structure of the sources: FR II sources are filled circles, FR I sources are open circles, and filled triangles denote core sources dominated by an unresolved central source. Values of $N_{0.5}$ for Abell richness 0, 1, and 2 clusters are indicated by A0, A1, and A2.

Analogous trends are also seen in terms of radio power, but the difference is more significant for the FR II sources alone because of the exclusion of low-redshift FR I sources which are above the RLF break, but which lie in rich environments. For radio powers between the RLF break at $10^{25.3}$ (indicated by a horizontal dotted line in Fig. 8) and 10^{27} W Hz^{-1} , the $z \sim 0.5$ sources are found in a wider range of environments, including many rich clusters which rarely if ever contain a powerful source at low redshift. A single-tailed U -test shows that in this power range, $z \sim 0.5$ radio galaxies inhabit richer environments than their low-redshift counterparts (99.8% confidence). For $z \sim 0.5$ sources with powers above the RLF break, there is no dependence of radio power on cluster environment, and if all the $z \sim 0.5$ sources above the RLF break are considered, including the ultrapowerful 3C sources, the significance of the difference in environments for sources above the RLF break increases to 99.9%. Figure 9 presents histograms of the cluster richness distributions for FR I and FR II sources from the low- and high-redshift samples.

The average richness of clusters associated with radio sources above the RLF break with powers $< 10^{27}$ W Hz^{-1} increases by a factor of about 2.5 from $N_{0.5} = 6$ –15 between $z \sim 0$ and 0.5. Powerful radio sources at $z \sim 0.5$ inhabit Abell richness class 0 clusters on average. It should be noted that there are no large negative values of $N_{0.5}$ in the $z \sim 0.5$ data and that the scatter of points to negative values is consistent with the Poisson errors stated above.

Figure 9 indicates that the distributions of environmental richness of FR I sources are very similar at both epochs. Two-tailed U -tests confirm that there is no detectable difference in the range and distribution of cluster environments for sources with FR I radio morphology or for those with powers below the break in the RLF between the two epochs. At low redshift, there are several quite powerful FR I sources in cluster environments, but such sources are absent at $z \sim 0.5$. This may

be related to the appearance of FR II sources in clusters at the earlier epoch.

Figure 10 shows that there is no significant correlation between the metric absolute B magnitudes of the radio galaxies and their environments. In this figure the radio galaxies are classified in terms of their radio structure. The quasars and the galaxies 1104+36, and 3C 299 have been excluded from this figure because of their nonthermal continua. The three 5C12 sources with $z > 0.6$ have also been excluded as these redshifts are not certain. Photometry of the radio galaxies shows that the absolute magnitudes of those found in clusters are consistent with their being the first-ranked cluster members, and this is in many cases confirmed by visual inspection of the images. Hence, 3C 295, which is associated with the first-ranked galaxy of an Abell richness class 0–1 cluster, is quite typical of radio galaxies with powers above the RLF break at $z \sim 0.5$.

b) Comparisons with Previous Results

i) Radio Galaxies

In a contemporaneous study, Yates, Miller, and Peacock (1989) have observed a largely independent sample of 25 3C and Parkes radio galaxies with flux densities > 1 Jy and redshifts between $z = 0.15$ and 0.6. There are only 11 sources at $z > 0.35$, and the use of essentially a single flux density-limited sample means that only a narrow range of the most luminous galaxies are studied at each redshift. Yates, Miller, and Peacock (1989) employed Yee and Green's (1987) evolving galaxy luminosity function to calculate B_{gg} values.

Despite the difficulties of observing this wide range of redshifts through a single passband and with a camera of limited field of view, Yates, Miller, and Peacock (1989) found that the most luminous sources at $z > 0.3$ lie in rich environments, typically of Abell richness class 0. The present sample confirms this with an independent data set. Transforming the B_{gg} values of Yates, Miller, and Peacock (1989) to $N_{0.5}$ using the empirical

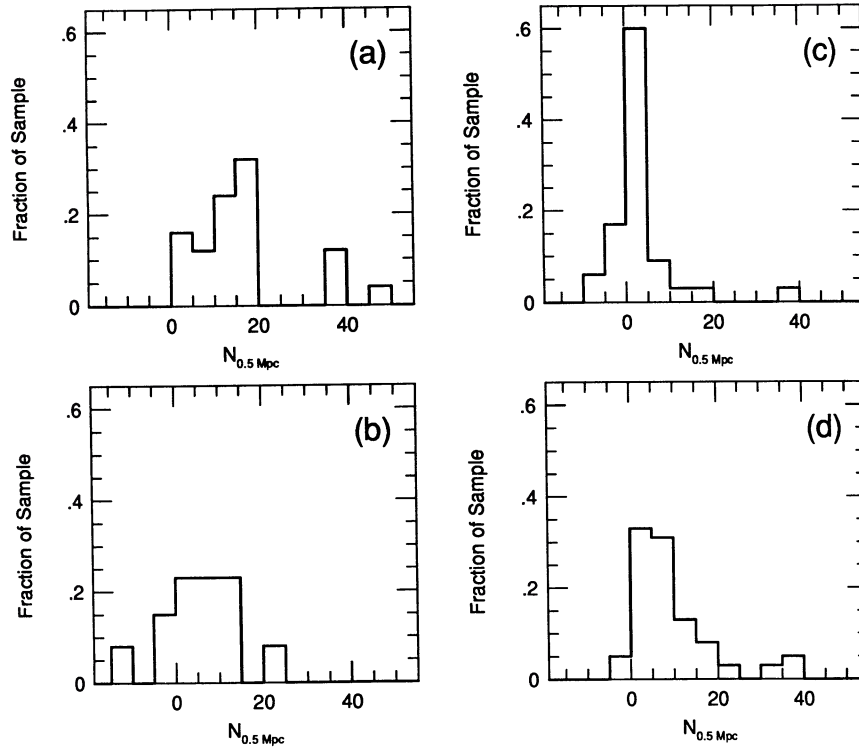


FIG. 9.—Histograms of the distribution of environmental richness for radio galaxies of different redshift and radio morphology. (a) $z \sim 0.5$, FR II; (b) $z \sim 0.5$, FR I; (c) $z \sim 0$, FR II; (d) $z \sim 0$, FR I.

calibration derived earlier, they find a mean $N_{0.5}$ for the redshift range $0.35 < z < 0.55$ of 8.1 ± 4.0 , to be compared with our 9.7 ± 1.5 (all sources) and 11.4 ± 3.2 (3C alone).

Yates, Miller, and Peacock (1989) were unable to satisfactorily address whether the change from $z = 0$, where luminous radio sources almost invariably avoid such rich environments,

was primarily due to the earlier epoch or to the much higher power of the high-redshift systems, since they had only a small dynamic range in power. Although a bivariate correlation analysis marginally supported an epoch dependence, Yates, Miller, and Peacock (1989) favored a straightforward power dependence, independent of epoch, because of an earlier sta-

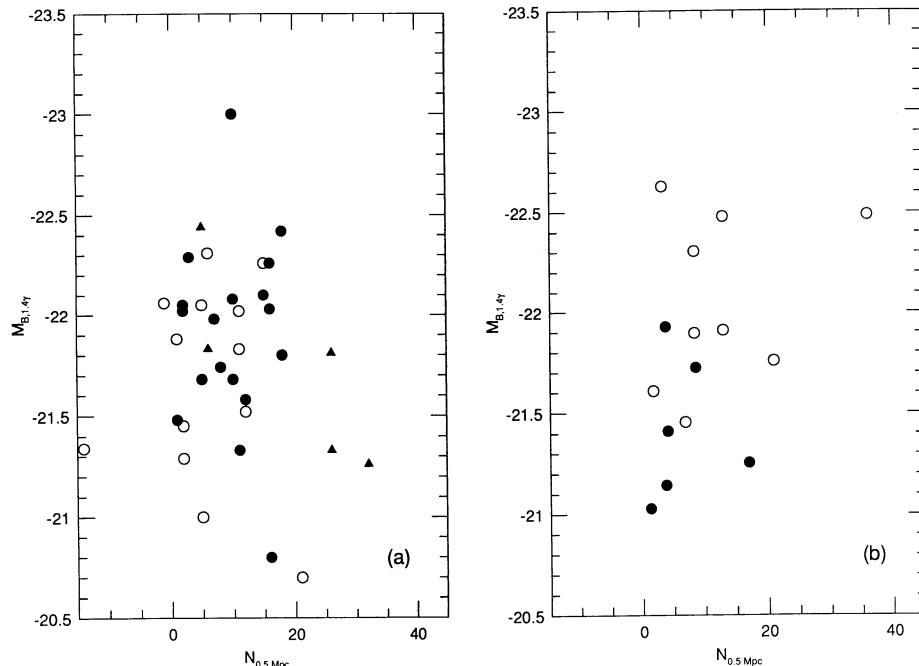


FIG. 10.—Metric absolute rest frame B magnitudes of radio galaxies as a function of cluster richness for (a) the $z \sim 0.5$ sample and (b) the low-redshift Lilly and Prestage (1987) subsample. The symbols are the same as in Fig. 8.

tistical analysis of Lilly and Longair's (1984) K - z relation (Yates, Miller, and Peacock 1987). In their picture, the richness power curve defined by the low-redshift sources in Figure 8b would curl up and to the right to pass through the most luminous sources in Figure 8a. This is because, as sources attain higher beam power, they are able to sustain double-lobe structure even in rich high-pressure environments.

By incorporating a wide range of luminosities at $z = 0.5$, the present investigation is able to unambiguously separate the effects of power and redshift and is able to show that epoch is a significant, and probably the dominant, effect. In particular, the 1 Jy and 5C sources at $z = 0.5$, which have powers that are similar to the most powerful sources at low redshift (but excluding the exceptional source Cygnus A), also occupy the richer environments. Indeed, there is no correlation of power and richness within our sample above $\log(P_{2.0}) = 25.3$.

ii) Quasars

Yee and Green (1984, 1987) have reported observations of the cluster environments of steep-spectrum, radio-loud quasars at redshifts up to $z \sim 0.6$, which are in principle directly comparable to those reported here for radio galaxies. The B_{gg} values of Yee and Green (1987) were transformed to values of $N_{0.5}$ assuming our "empirical" calibration as at low redshift. In Figure 11, we have plotted our radio galaxies and Yee and Green's quasars as a function of redshift. For the redshift range $0.35 < z < 0.6$, a two-tailed U -test shows that quasars and radio galaxies with similar radio properties inhabit the same range of cluster environments, within the statistics of the samples. It should be noted that Yee and Green were unable to study the changes between $z = 0.5$ and 0.0 that are the main subject of this paper because of the paucity of low-redshift quasars but had a larger range of redshifts (up to $z = 0.65$) at the high-redshift end.

Yee and Green (1987), however, do present evidence for a sudden increase of about a factor of 3 in quasar cluster richness between $z \sim 0.4$ and 0.6 . The small redshift range of our radio galaxy sample is insufficient (with few sources at $z > 0.5$) to definitively address whether the radio galaxies show a similar effect. Transforming Yee and Green's B_{gg} values to $N_{0.5}$ as before, their mean values at $0.35 < z < 0.55$ and $0.55 < z < 0.65$ of 4.4 ± 2.0 and 14.0 ± 4.5 , respectively, strad-

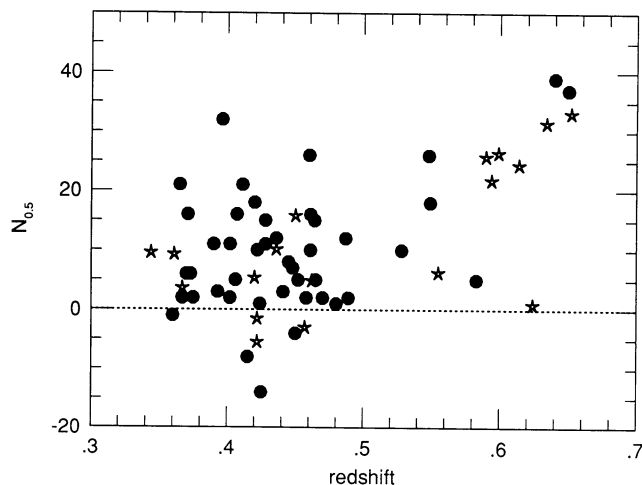


FIG. 11.—Comparison of the cluster environments of Yee and Green's (1987) quasars (stars) and the radio galaxies in this study (filled circles).

dle the radio galaxy value at $0.35 < z < 0.55$ of around 8–10 (previous section). If the change in quasar densities on a time scale of only 1.5 Gyr is confirmed by more extensive samples and if it is not found in the radio galaxy data at higher redshifts, then it will be interesting for two reasons. First, it would be incompatible with the unification of the two classes through orientation effects (e.g., Barthel 1989). Second, it would indicate that rich environments became inhospitable for radio quasars earlier than for radio galaxies.

c) The Cosmic Evolution of the Radio Source Population

The systematic change in environment with redshift may have important consequences for the cosmological evolution of the radio source population. We discuss two of these in this section.

First, the change allows us to address the question of the extent to which the physical cause of the RSP evolution (Fig. 1) should be regarded as luminosity evolution or differential density evolution. In this context, luminosity evolution implies that a fixed population of radio sources is seen in which all sources fade at the same rate, this fading either being a continuous process or, more likely, a diminishment of the luminosity of individual outbursts. In contrast, differential density evolution implies an epoch-dependent chance of a given object being a radio galaxy of a given power. It is therefore a less constrained scenario with more free parameters. The shape of the break in the RLF means that pure luminosity evolution can have the same effect on the epoch-dependent RLF as differential density evolution. The curves in Figure 1 are fits to the available RLF data from Peacock (1985) and are poorly constrained at low powers for the $z \sim 0.5$ curve (due to the lack of faint identified radio surveys and at high power at low redshift (due to the scarcity of sources). Hence, the available RLF data cannot distinguish between pure luminosity evolution and differential density evolution.

The results of this investigation are clearly consistent with density evolution, and in fact they strongly suggest that the RSP evolution should not be regarded as pure luminosity evolution (e.g., Condon 1984) over the past 6 Gyr. This is because the richness of a given cluster is very unlikely to decrease with time. Consequently, the luminous 3C and 1 Jy radio sources at $z \sim 0.5$ in rich environments must fade by one to two orders of magnitude by the present epoch to be seen as low-luminosity FR I sources. This is much larger than the implied dimming of a factor of 3 (applied uniformly to all sources) on Figure 1.

In terms of an explanation of differential density evolution, an intriguing possibility is suggested by the data. It was remarked above that the low-power sources, which show little density enhancement between the two epochs, have not shown a significant change in environment, either. In contrast, the more powerful sources, which do show significant density enhancements over this time scale, are also the ones where the typical environment has altered. An interesting question is therefore to ask what is the richness of the "excess sources," over and above the low-redshift RLF, at $z \sim 0.5$. This is shown in Figure 12, where we have plotted histograms of the cluster richnesses of sources of different power at $z = 0$ and $z = 0.5$, and the difference between these to represent this excess. The bin width is 10 galaxies, and these histograms have all been normalized to the number density of low-redshift sources in each power bin. It is evident in this figure that the excess sources at high redshift (in the right-hand bin) are preferentially in much richer environments than their low-redshift

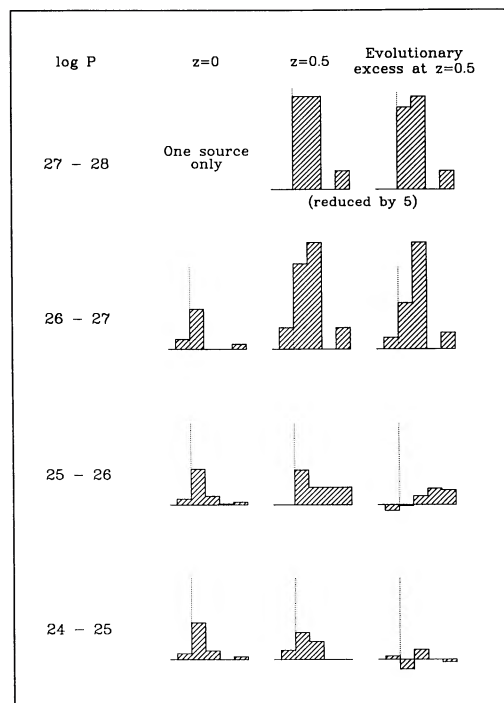


FIG. 12.—The distribution of environments at $z \sim 0$ and $z \sim 0.5$ as a function of radio power. The histograms are normalized to the number of sources in the zero-redshift sample (i.e., the first column) in each power range. The number of objects in each histogram in the second column at $z \sim 0.5$ is larger by the evolutionary factor shown in Fig. 1 for each power interval. The third column represents the difference between these histograms and may be thought of as the evolutionary excess at $z \sim 0.5$. These last histograms are consistent with the idea that all of the excess sources are located in rich environments. Statistical uncertainties in each object correspond to roughly one bin.

counterparts. Remembering that the statistical uncertainty in each individual measurement is approximately one bin on Figure 12, the data are consistent with a constant number of sources in poor environments, with essentially all of the evolutionary excess coming from sources in rich (Abell 0 or more) clusters.

We therefore suggest, as a speculation that is consistent with the data, that, to $z \sim 0.5$, the evolution in the radio source population may be accounted for entirely by an increase in the availability of “rich” sites capable of sustaining a high-luminosity source. The steepness of the RLF and the correspondingly large numbers of present-day low-luminosity FR I sources in rich Abell 0 clusters offers a ready explanation of the fate of these luminous sources. This picture thus has drastic luminosity evolution for those luminous sources that are in rich environments at high redshift. As the environments evolve, they are unable to sustain FR II sources below a certain threshold, and the counterparts to these sources may be seen today as FR I low-luminosity systems. Even if correct, this cannot be the whole story, as it fails to explain why the most powerful FR II’s have evolved more than the less powerful FR II’s.

d) An Evolution in the Intracluster Medium?

Where obvious clusters are present around the radio galaxies, visual inspection of the images shows that the radio sources are associated with the first-ranked cluster members. The absolute magnitudes of the galaxies (Figs. 5 and 8) are also

consistent with those expected for first-ranked objects. Thus, the evolution seen in the cluster environments of powerful radio sources may be the result of evolution of the properties of first-ranked cluster ellipticals.

Regardless of the validity of the scenario for the RSP evolution presented in the previous section, the 1 Jy and 5C12 sources in clusters at $z \sim 0.5$ have the same power as sources at low redshift which avoid such clusters. Some property of the clusters or their central galaxies must have changed over the past 6 Gyr to significantly affect their ability to generate a powerful FR II radio source. As discussed above, the disruption of jets may explain why FR II sources do not survive in clusters at low redshift. An attractive possibility is that the IGM pressure was lower in some clusters at the earlier epoch. This observation can be explained if these $z \sim 0.5$ galaxies have environments more characteristic of those of isolated or group giant ellipticals found at low redshift.

The latest determination of the X-ray luminosity function of clusters at $z \sim 0.5$ suggests that some evolution may be occurring in the sense that the most X-ray luminous clusters have a higher space density now than they did in the past (Gioia *et al.* 1990). This may be due to an increase in IGM density with time. A lower IGM density at earlier epochs is consistent with models of cluster evolution (e.g., Perrenod 1978) and would support previous ideas of possible mechanisms for the RSP evolution. Stocke and Perrenod (1981), De Robertis (1985), and Roos (1985) have presented scenarios in which the increase in IGM density as clusters evolve, or the increase in velocity dispersion upon virialization, make the triggering of nuclear activity in cluster galaxies less probable as time passes.

V. SUMMARY

The cluster environments of a sample of 45 $z \sim 0.5$ radio galaxies have been studied and compared with those of their low-redshift counterparts of the same radio power. It is found that the high-redshift, powerful radio sources (above the break in the RLF) are found on average in richer environments than at low redshift. Lower power sources below the break in the RLF show no change in environment between the epochs. It is suggested that the change in available sites for powerful radio sources may be of fundamental significance in understanding the cosmic evolution of the radio source population. An increase in the density of the intergalactic medium in clusters since $z \sim 0.5$ may provide a physical explanation for the change in environment. The *B* band absolute magnitudes of both the radio galaxies and of cluster *L** galaxies show no significant change relative to their low redshift values. The cluster environments of radio galaxies and of radio-loud quasars appear to be the same at $z \sim 0.5$.

The referee, Howard Yee, made several suggestions which significantly improved the presentation of this paper. Chris Benn and Rogier Windhorst provided valuable information on identifications in advance of publication. We also gratefully acknowledge discussions with Len Cowie, Richard Green, Pat Henry, Esther Hu, Pat Leahy, John Peacock, and Alan Stockton. We thank the staffs of the University of Hawaii 2.2 m telescope, the University of Texas McDonald Observatory, and the VLA for their assistance in obtaining the data on which this paper is based. The GASP data reduction package was written by M. Cawson and was implemented at the Institute for Astronomy by M. J. Pierce. G. J. H. acknowledges

support from a McDonald Fellowship at the University of Texas, during the preparation of this manuscript and the final stages of the observational program. This work was supported

by NSF grant AST-8718275. Implementation of the CCD camera at the Institute for Astronomy was supported by NSF grant AST-8615631.

REFERENCES

- Abell, G. O. 1958, *Ap. J. Suppl.*, **3**, 211.
 Allington-Smith, J. R., Lilly, S. J., and Longair, M. S. 1985, *M.N.R.A.S.*, **213**, 243.
 Allington-Smith, J. R., Spinrad, H., Djorgovski, S., and Leibert, J. 1988, *M.N.R.A.S.*, **234**, 1091.
 Bahcall, J. N., and Soneira, R. M. 1984, *Ap. J. Suppl.*, **55**, 67.
 Bahcall, N. A. 1981, *Ap. J.*, **247**, 787.
 Barthel, P. D. 1989, *Ap. J.*, **336**, 606.
 Benn, C. R., Grueff, G., Vigotti, M., and Wall, J. V. 1988, *M.N.R.A.S.*, **230**, 1.
 Broadhurst, T. J., Ellis, R. S., and Shanks, T. 1988, *M.N.R.A.S.*, **235**, 827.
 Butcher, H., and Oemler, A., Jr. 1978, *Ap. J.*, **219**, 18.
 ———. 1984, *Ap. J.*, **285**, 426.
 Coleman, G. D., Wu, C.-C., and Weedman, D. W. 1980, *Ap. J. Suppl.*, **43**, 393.
 Colless, M., Ellis, R. S., Taylor, K., and Hook, R. N. 1990, *M.N.R.A.S.*, **244**, 408.
 Condon, J. J. 1984, *Ap. J.*, **284**, 44.
 Dahari, O. 1984, *A.J.*, **89**, 966.
 Davis, L. E., Cawson, M. E., Davies, R. L., and Illingworth, G. 1985, *A.J.*, **90**, 169.
 De Robertis, M. 1985, *A.J.*, **90**, 998.
 de Vaucouleurs, G., and Capaccioli, M. 1979, *Ap. J. Suppl.*, **40**, 699.
 Dressler, A., Gunn, J. E., and Schneider, D. P. 1985, *Ap. J.*, **294**, 70.
 Eales, S. A. 1985, Ph.D. thesis, University of Cambridge.
 Ellis, R. 1983, in *The Origin and Evolution of Galaxies*, ed. B. J. T. and J. E. Jones (Dordrecht: Reidel), p. 225.
 Fanaroff, B. L., and Riley, J. M. 1974, *M.N.R.A.S.*, **167**, 31p.
 Felton, J. E. 1977, *A.J.*, **82**, 861.
 Gioia, I. M., Henry, J. P., Maccacaro, T., Morris, S. L., Stocke, J. T., and Wolter, A. 1990, *Ap. J.* submitted.
 Gunn, J. E., and Oke, J. B. 1975, *Ap. J.*, **195**, 255.
 Heckman, T. M., Bothun, G. D., Balick, B., and Smith, E. P. 1984, *A.J.*, **89**, 958.
 Heckman, T. M., Smith, E. P., Baum, S. A., van Breugel, W. J. M., Miley, G. K., Illingworth, G. D., Bothun, G. D., and Balick, B. 1986, *Ap. J.*, **311**, 526.
 Hine, R. G., and Longair, M. S. 1979, *M.N.R.A.S.*, **188**, 111.
 Hintzen, P., Ulvestad, J., and Owen, F. 1983, *A.J.*, **88**, 709.
 Horne, K. 1986, *Pub. A.S.P.*, **98**, 609.
 Hutchings, J. B., Crampton, D., and Campbell, B. 1984, *Ap. J.*, **280**, 41.
 King, C. R., and Ellis, R. S. 1985, *Ap. J.*, **288**, 456.
 Kron, R. G., Koo, D. C., and Windhorst, R. A. 1985, *Astr. Ap.*, **146**, 38.
 Kuhr, H., Witzel, A., Pauliny-Toth, I. I. K., and Naber, U. 1981, *Astr. Ap. Suppl.*, **45**, 367.
 Laing, R. A., Riley, J. M., and Longair, M. S. 1983, *M.N.R.A.S.*, **204**, 151.
 Landolt, A. U. 1983, *A.J.*, **88**, 439.
 Lavery, R. J., and Henry, J. P. 1988, *Ap. J.*, **330**, 596.
 Lilly, S. J. 1987, *M.N.R.A.S.*, **229**, 573.
 ———. 1989, in *The Evolution of the Universe of Galaxies: The Edwin Hubble Centennial Symposium*, ed. R. Kron (*A.S.P. Conf. Ser.*, **10**), in press.
 Lilly, S. J., and Longair, M. S. 1984, *M.N.R.A.S.*, **211**, 833.
 Lilly, S. J., McLean, I. S., and Longair, M. S. 1984, *M.N.R.A.S.*, **209**, 401.
 Lilly, S. J., and Prestage, R. M. 1987, *M.N.R.A.S.*, **225**, 531.
 Longair, M. S. 1966, *M.N.R.A.S.*, **133**, 421.
 Longair, M. S., and Riley, J. M. 1979, *M.N.R.A.S.*, **188**, 625.
 Longair, M. S., and Seldner, M. 1979, *M.N.R.A.S.*, **189**, 433.
 MacKenty, J. W. 1989, *Ap. J.*, **343**, 125.
 Mann, H. B., and Whitney, D. R. 1947, *Ann. Math. Statistics*, **18**, 52.
 Oort, M. J. A., Katgert, P., Steeman, F. W. M., and Windhorst, R. A. 1987, *Astr. Ap.*, **179**, 41.
 Oke, J. B., and Gunn, J. E. 1983, *Ap. J.*, **266**, 713.
 Owen, F. N., and Laing, R. A. 1989, *M.N.R.A.S.*, **238**, 357.
 Peacock, J. A. 1985, *M.N.R.A.S.*, **217**, 601.
 Peacock, J. A., and Wall, J. V. 1981, *M.N.R.A.S.*, **194**, 331.
 Perrenod, S. C. 1978, *Ap. J.*, **226**, 566.
 Prestage, R. M., and Peacock, J. A. 1988, *M.N.R.A.S.*, **230**, 131.
 ———. 1989, *M.N.R.A.S.*, **236**, 959.
 Roos, N. 1985, *Ap. J.*, **294**, 486.
 Sandage, A. 1973, *Ap. J.*, **183**, 731.
 Schechter, P. 1976, *Ap. J.*, **203**, 297.
 Schneider, D. P., Gunn, J. E., and Hoessel, J. G. 1983, *Ap. J.*, **268**, 476.
 Seldner, M., and Peebles, P. J. E. 1978, *Ap. J.*, **225**, 7.
 Seldner, M., Seibers, B., Groth, E. J., and Peebles, P. J. E. 1977, *A.J.*, **82**, 242.
 Shane, C. D., and Wirtanen, C. A. 1967, *Pub. Lick Obs.*, **22**, Part 1.
 Smith, E. P., and Heckman, T. M. 1989, *Ap. J.*, **341**, 658.
 Spinrad, H., Djorgovski, S., Marr, J., and Aguilar, L. 1985, *Pub. A.S.P.*, **97**, 932.
 Spinrad, H., and Stauffer, J. R. 1982, *M.N.R.A.S.*, **200**, 153.
 Stocke, J., and Perrenod, S. C. 1981, *Ap. J.*, **245**, 375.
 Stockton, A. 1978, *Ap. J.*, **223**, 747.
 ———. 1982, *Ap. J.*, **257**, 33.
 Stone, R. P. S. 1977, *Ap. J.*, **218**, 767.
 Stover, R. J. 1988, in *Instrumentation for Ground Based Optical Astronomy*, ed. L. B. Robinson (New York: Springer), p. 443.
 Tyson, J. A. 1988, *A.J.*, **96**, 1.
 Wall, J. V. 1977, in *IAU Symposium 74, Radio Astronomy and Cosmology*, ed. D. L. Jauncey (Dordrecht: Reidel), p. 55.
 Windhorst, R. A., Kron, R. G., and Koo, D. C. 1984, *Astr. Ap. Suppl.*, **58**, 39.
 Yates, M. G., Miller, L., and Peacock, J. A. 1987, *M.N.R.A.S.*, **221**, 311.
 ———. 1989, *M.N.R.A.S.*, **240**, 129.
 Yee, H. K. C., and Green, R. F. 1984, *Ap. J.*, **280**, 79.
 ———. 1987, *Ap. J.*, **319**, 28.
 Zwicky, F., Herzog, E., Wild, P., Karpowicz, M., and Kowal, C. T. 1961–1968, *Catalogue of Galaxies and Clusters of Galaxies* (Pasadena: California Institute of Technology).

GARY J. HILL: McDonald Observatory, University of Texas at Austin, RLM 15.308, Austin, TX 78712-1083

SIMON J. LILLY: Institute for Astronomy, University of Hawaii at Manoa, 2680 Woodlawn Drive, Honolulu, HI 96822